Holocene vegetation dynamics in response to climate change and hydrological processes in the Bohai region

Chen Jinxia[a,b,*], Shi Xuefa[a,b,*], Liu Yanguang[a,b], Qiao Shuqing[a,b], Yang Shixiong[c,d], Yan Shijuan[a,b], Lv Huahua[a,b], Li Jianyong[e,f], Li Xiaoyan[a,b], Li Chaoxin[a,b]

[a] Key Laboratory of Marine Geology and Metallogeny, First Institute of Oceanography, MNR, Qingdao 266061, China

[b] Laboratory for Marine Geology, Pilot National Laboratory for Marine Science and Technology, Qingdao 266061, China

[c] Key Laboratory of Coastal Wetland Biogeosciences, China Geological Survey, Qingdao 266071, Shandong, China

[d] Laboratory for Marine Geology, Qingdao National Laboratory for Marine Science and Technology, Qingdao, 266061, China

[e] Shanxi Key Laboratory of Earth Surface System and Environmental Carrying Capacity, College of Urban and Environmental Sciences, Northwest University, Xi'an, China

[f] Institute of Earth Surface System and Hazards, College of Urban and Environmental Sciences, Northwest University, Xi'an, China,

[*] Corresponding author at: Key Laboratory of Marine Geology and Metallogeny, First Institute of Oceanography, MNR, Qingdao 266061, China.

E-mail address: jinxiachen@fio.org.cn (J. Chen); xfshi@fio.org.cn (X. Shi).

ABSTRACT

Coastal vegetation both mitigates the damage inflicted by marine disasters on coastal areas and plays an important role in the global carbon cycle (i.e. blue carbon). Nevertheless, detailed records of changes in coastal vegetation composition and diversity in the Holocene, coupled with climate change and river evolution, remain unclear. To explore vegetation dynamics and their influencing factors on the coastal area of the Bohai Sea (BS) during the Holocene, we present high-resolution pollen and sediment grain size data obtained from a sediment core of the BS. The results reveal that two rapid and abrupt changes in salt marsh vegetation are linked with the river-system changes. Within each event, a recurring pattern—starting with a decline in Cyperaceae, followed by an increase in *Artemisia* and Chenopodiaceae—suggests a successional process that is determined by the close relationship between Yellow River (YR) channel shifts and the wetland community dynamics. The phreatophyte Cyperaceae at the base of each sequence indicate lower saline conditions. Unchannelized river flow characterized the onset of the YR channel shift, caused a huge river-derived sediment accumulation in the floodplain, and destroyed the sedges in the coastal depression. Along with the formation of a new channel, lateral migration of the lower channel stopped, and a new intertidal mudflat was formed. Pioneer species (Chenopodiaceae, *Artemisia*) were the first to colonize the bare zones of the lower and middle marsh areas. In addition, the pollen

33 results revealed that the vegetation of the BS land area was dominated by broadleaved forests during

34 the early Holocene (8500–6500 a BP) and by conifer and broadleaved forests in the middle Holocene

35 (6500–3500 a BP), which was followed by an expansion of broadleaved trees (after 3500 a BP). The

36 pollen record indicated that a warmer early and late Holocene and colder middle Holocene were

37 consistent with previously reported temperature records for East Asia. The main driving factors of

38 temperature variation in this region are insolation, the El Niño-Southern Oscillation and greenhouse

39 gases forcing.

40

42

1. Introduction

44   Coastal areas, where cities, populations and industries are clustered, are playing an increasingly

45 critical role in trade globalization (Hemavathi et al., 2019). Because they are located between marine

46 ecosystems and terrestrial ecosystems, coastal areas are prone to many natural hazards such as

47 flooding, storms, and tsunamis (Hou and Hou, 2020). Coastal vegetation, which acts as a natural

48 barrier, is widely distributed in coastal areas and could effectively mitigate the damage caused by

49 marine disasters to the economy and environment of coastal areas (Zhang et al., 2018). Moreover,

50 despite their relatively small global extent (between 0.5 and 1×10^6 km^2), coastal vegetation

51 ecosystems, tidal marshes, mangroves, and seagrasses play an important role in the global carbon

52 cycle (Serrano et al., 2019; Spivak et al., 2019). Per unit area, their organic carbon sequestration

53 rates exceed those of terrestrial forests by 1–2 orders of magnitude and contribute ~50% of carbon

54 sequestered in marine sediments (Serrano et al., 2019). Hence, it is important to understand the long-

55 term spatial–temporal dynamics of coastal vegetation, which are favorable for the global carbon

56 cycle research and coastal restoration.

57   Climatic fluctuation, post glacial sea-level rise and changes in river discharge provoked

58 dramatic habitat changes along coastal areas during the Late Pleistocene and Holocene (Neumann

59 et al., 2010; Cohen et al., 2012; Pessenda et al., 2012; França et al., 2015). Presently, the relationship

60 of sea-level change and coastal vegetation (especially mangrove) evolution has been widely studied

61 by many researchers (e.g. Engelhart et al., 2007; Gonza lez and Dupont, 2009; França et al., 2012;

62 Woodroffe et al., 2015; Hendy et al., 2016). Contrarily, studies on the long-term dynamics of coastal

63   vegetation, coupled with climate change and river evolution, are sparse. During the Holocene, the

64   global rivers delivered large amounts of material to the ocean, the total suspended sediment

65   delivered by all rivers to the ocean was approximately 13.5×10^9 tons annually (Milliman and

66   Meade, 1983). The material transported by the rivers had huge impacts on the coastal ecosystem.

67   Hence, a deeper understanding of correlations between coastal vegetation and river variables is

68   required to better assess coastal vegetation responses to global warming in the future.

69   In the coastal areas of the Bohai Sea (BS), vegetation is dominated by warm temperate

70   deciduous broadleaved forests and shrub grasslands (Wang et al., 1993). The Yellow River (YR), as

71   one of the largest river in the world in terms of sediment discharge (Milliman and Meade, 1983),

72   transports large amounts of sediment into the BS every year; hence, it has developed a delta complex

73   in the west coastal region of the BS since 7000 a BP (He et al., 2019). Deposition of the Yellow

74   River delta (YRD) complex resulted in the formation of a vast area of floodplain and estuarine

75   wetland (Xue et al., 1995; Cui et al., 2009; Liu et al., 2009b). Based on the study of coastal

76   vegetation of the BS, it is helpful to understand the spatial and temporal drivers of ecological

77   variability, and thus of the vegetation-climate and river relationship, especially wetland dynamics.

78   However, there have been few studies investigating the vegetation dynamics and their response to

79   climate and river variables in the Bohai region.

80   Pollen records have been useful in terms of reconstructing vegetation dynamics and

81   environmental changes associated with climatic changes in the geological record (Bao et al., 2007;

82   Cohen et al., 2008; Giraldo-Giraldo et al., 2018). In this study, we carried out a detailed investigation

83   of core sediments from Laizhou Bay, BS. We analyzed pollen and grain size proxies under high

84   resolution and refined the chronology of the core by ^{137}Cs and accelerator mass spectrometry

85   (AMS) ^{14}C dates. With this in mind, the specific objectives of the current research are formulated

86   as follows: (1) to reconstruct the vegetation evolution history in the Bohai region and (2) to

87   tentatively discuss the effects of climate and environment on coastal vegetation (especially wetlands)

88   during the Holocene.

89

90   **2. Study area**

91   **2.1. Geographical settings**

92   The BS, a shallow inland sea in China, is connected with the Yellow Sea through the narrow

93   Bohai Strait (Figure 1). The main rivers flowing into the BS are the YR, Haihe River, Luanhe River,

94   and Liaohe River. Among these, the YR is the largest and is the main source of sediments in this

95   region. Over the past 2000 years, the YR has annually provided approximately 1.1×10^9 tons of

96   sediment discharged into the BS (Milliman et al., 1987). This immense amount of sediment has

97   resulted in the rapid seaward progradation of YRD, and a rapid change in the location of the main

98   distributaries in the lower delta plain.

99   The tidal current plays a critical role in the transportation and distribution of sediments in the

100   BS. The tidal currents of the modern BS are dominated by semi-diurnal tides. The velocity of tidal

101   currents varies from 20 to 80 cm/s. Three strong tidal current areas are observed in the northern

102   Bohai Strait, the central part of Bohai Bay, and the eastern part of Liaodong Bay (Huang et al., 1999).

103   In Laizhou Bay close to the core location, the speed of tidal currents is weak (Gu and Xiu, 1996).

104   The wind waves off the YRD are dominated by the East Asian monsoon and show significant

105   seasonal variations. The prevailing northerly winds are much stronger in winter than the dominant

106   southerly winds in summer. Strong winter winds cause strong wind waves, and thus strong bottom

107   shear stresses which readily erode seabed sediment into water (Yang et al., 2011; Wang et al., 2014;

108   Zhou et al., 2017).

109   The circulation of the BS is weak, and the mean flow velocity is small. In winter, the

110   predominant extension of the Yellow Sea Warm Current (YSWC) intrudes and crosses the Bohai

111   Strait, moving westward along the central part of the BS and splits into two branches. One branch

112   moves toward the northeast to form a clockwise gyre (Liaoxi Coastal Current [LXCC]), and the

113   other veers southward and then turns eastward along the southern coast to form a counterclockwise

114   gyre (Libei Coastal Current [LBCC]). In summer, the YSWC disappears in the BS, and eddies

115   generated in the BS are stronger than in winter. During this time, the central eddy is missing, the

116   eddy in Laizhou Bay is more pronounced, and the coastal current along the southern and western

117   coastlines of the BS is established (Figure 2; Liu et al., 2015; Yang et al., 2016).

118

119   **2.2. Climate and vegetation**

120   The Bohai region lies in a zone of warm temperate monsoonal climate with distinctive seasons.

121   The annual mean air temperature is 9.5–13.1 ℃. The annual average precipitation is about 600 mm,

122   and 60–70% of the total annual precipitation occurs between June and August (Qiao et al., 2012).

123 As the Liaodong Peninsula and Shandong Peninsula protrude into the sea, they are clearly

124 influenced by its proximity and experience sufficient rainfall. There is less rainfall in the mountain

125 area of the northern part (Wang et al., 1993).

126 The regional vegetation is dominated by warm temperature deciduous broadleaved forests and

127 shrub grasslands. Currently, natural vegetation only remains in the mountain areas because of

128 widespread anthropogenic activities (e.g. cultivation and farming). The predominant deciduous

129 broadleaved species belong to *Quercus*, such as *Q. liaotungensis*, *Q. dentata, Q. acutissima*, and *Q.*

130 *mongolica*. Co-dominant plants are *Pinus*, including *P. densiflora* that grows in the coastal humid

131 area, and *P. tabuliformis* that is distributed in the relatively dry North China plain. In the plain area,

132 apart from *P. tabuliformis*, there are some deciduous broadleaved trees, such as *Ailanthus altissima*,

133 *Koelreuteria paniculata*, and *Morus alba*. Other broadleaved trees, *Betula ermanii*, *Populus tremula*,

134 *Acer* spp., *Tilia amurensis*, and *Carpinus turczaninowii* are distributed in the hills and lowlands

135 (Wang et al., 1993). The coastal wetlands are occupied by herbs and shrubs, such as *Tamarix*

136 *chinensis*, *Salix matsudana*, *S. integra*, *Phragmites australis*, *Aeluropus*, *Limonium sinense*, *Suaeda*

137 *glauca*, *Typha orientalis*, and *Acorus calamus* (Wang et al., 1993; Li et al., 2007; Xu et al., 2010).

138

139 **3. Materials and methods**

140 **3.1. Coring, sub-sampling, and chronology**

141 Core CJ06-435 was collected in Laizhou Bay, BS in August 2007 by the R/V *Kan407* of the

142 Shanghai Bureau. The core site is located at 37.50 °N, 119.52 °E, at a water depth of 14.6 m (Figure

143 1); the core had a length of 271 cm. In the laboratory, the core was spilt into two sections,

144 photographed, macroscopically described, and sub-sampled.

145 Isotopes ^{137}Cs and ^{210}Pb were measured employing EG&G Ortec Gamma Spectrometry at the

146 Nanjing Institute of Geography and Limnology, Chinese Academy of Sciences (NIGLAS). The

147 sediment samples were air-dried and pulverized. [137]Cs and ^{210}Pb concentrations were then

148 determined from gamma emissions at 662 and 46.5 keV, respectively. In addition, a total of 10

149 samples consisting of foraminifera were obtained from the core for radiocarbon dating. The

150 radiocarbon dating was conducted at the Woods Hole Oceanographic Institution (WHOI) and Beta

151 Analytic Inc., USA. Radiocarbon dates were corrected for the regional marine reservoir effect (ΔR

152 = −139 ± 59 years, a regional average value determined for the BS) and calibrated using the Calib

153   7.04 program (Stuiver et al., 2019) with one standard deviation uncertainty ($1.0 \times \sigma$) (Table 1).

154

155   **3.2. Palynological and sediment grain size sample analysis**

156   A total of 127 samples were selected for pollen analyses. Each sample was oven-dried at 60 ℃

157   for 24 h. The dry-weight of the samples ranged from 2.5 g to 13.9 g. Samples were chemically

158   treated according to the procedure outlined by Faegri and Iversen (1992). Before treatment, a

159   standard tablet of *Lycopodium* spores (mean=18,583±764 spores per tablet) was added to each

160   sample to aid in the calculation of palynological concentrations. Samples were treated with 15%

161   HCl solution to remove carbonates, boiled in 10% KOH solution for 5 min to remove humic acids,

162   then treated with 40% HF to remove silicates. The residue was mounted in glycerin jelly. Fossil

163   pollen was identified and counted with a light microscope at $400\times$ magnification. A minimum of

164   200 pollen grains were counted for each sample. The palynological concentrations of per gram

165   sediment (PCP) were calculated using the follow equation:

166
$$PCP = \frac{18583}{Lycopodium \text{ number per slide}} * \frac{\text{Pollen or Spore Counts per slide}}{\text{Net weight of dry sample}}$$

167   The percentage of each pollen type was calculated from the total sum of pollen and spores.

168   The pollen diagram was produced using the Tilia program, and the pollen assemblage zones were

169   divided based on the results of a constrained cluster analysis (CONISS) within Tilia (Grimm, 1987).

170   Analysis of sediment grain size was performed at 2.0 cm intervals throughout the core using

171   a Malvern Mastersizer 2000 instrument at the laboratory of the First Institute of Oceanography. The

172   chemical procedure of grain size experimental pretreatment was consistent with the procedures

173   described by Chen et al. (2019a). A solution of 30% H_2O_2 and 1.0 mol/L HCl were added to

174   decompose the organic matter and remove carbonates.

175

176   **4. Results**

177   **4.1. Chronological model**

178   Measurements of ^{137}Cs and ^{210}Pb revealed activity at the top of the profile, indicating the

179   recovery of recently deposited sediments. [137]Cs is a bomb-derived radionuclide, first appearing in

180   environmental samples at measurable levels around 1954 with the onset of nuclear weapon testing

181   (Kirchner and Ehlers, 1998), and was most prevalent in 1963 (the year of maximum fallout from

182 atmospheric weapon testing) (Palinkas and Nittrouer, 2007). Sub-surface peaks are not discernible

183 in ^{137}Cs profiles of core CJ06-435 (Figure 3). However, the deepest onset of ^{137}Cs is an effective

184 marker of the year 1954 (25 cm).

185   Often, the combined data of ^{137}Cs and excess ^{210}Pb have been used to calculate the

186 sedimentation rates (Wu et al., 2015). Excess ^{210}Pb shows a downward decline owing to the decay

187 of ^{210}Pb when the sediment stably accumulates for an appropriate period, and the excess [210]Pb

188 activity could be used to calculate the sedimentation rate. However, the excess ^{210}Pb profiles of core

189 CJ06-435 did not show a clear downward decline trend (Figure 3), and excess ^{210}Pb in the upper

190 parts of the core is not that large when compared with the lower background values. Thus, the [210]Pb

191 data seemed to be unsuitable for estimating the sedimentation rate of core CJ06-435. The [137]Cs–

192 derived average sedimentation rate was 0.47 cm/yr in the upper 25 cm of core CJ06-435.

193   The results of AMS radiocarbon dating are shown in Table 1 and Figure 3. Three samples

194 above the 20 cm depth were not included in the age model because their ^{14}C age was anomalously

195 greater than the ^{137}Cs dating. The dating point of 129 cm was eliminated because it appears not to

196 be reliable. According to the result of He et al. (2019), the calculated sedimentation rate (CSR) in

197 the tidal flat and neritic area of the south BS ranged from 0.02 to 0.13 cm/year before 2000 a BP

198 (calculation from cores H9601, H9602, ZK228, and ZK1, Figure 1). If the 129 cm dating is correct,

199 the CSR would be as high as 0.45 cm/yr in the section of 87–129 cm (4801–4894 a BP) for core

200 CJ06-435. It is apparently not reasonable because core CJ06-435 is offshore compared to the other

201 cores (e.g. H9601, H9602, ZK228, and ZK1, Figure 1) reported in previous researches (Xue et al.,

202 1988; Saito et al., 2000; Li et al., 2013). It should have a lower CSR compared to those cores rather

203 than an approximate ten-fold increase in CSR. The calibrated dates of several other samples are

204 plotted against sediment depth and shown in Figure 4.

205

206 **4.2. Sediment grain size distributions**

207   The grain size parameters and components percentages show distinct variations. The mean

208 grain size and the median grain size both show high values at depths of 271–160 cm, 135–83 cm

209 and 19–0 cm, lower values at a depth of 83–34 cm, and the lowest values at depths of 160–135 cm

210 and 34–19 cm. There was a smaller proportion of clay in the lower profile (271–160 cm) than in the

211 upper profile (160–0 cm, except for the two sections of 160–135 cm and 34–19 cm). The sequences

212 of silt and sand contents showed a strong inverse association. There were high proportions of silt

213 and low proportions of sand at depths of 271–222 cm, 180–160 cm, 135–83 cm, 40–34 cm and 19–

214 0 cm, lower proportions of silt and higher proportions of sand at depths of 222–180 cm and 83–40

215 cm, and the lowest proportions of silt and the highest proportions of sand occurred at depths of 160–

216 135 cm and 34–19 cm (Figure 3).

217

4.3. Palynology assemblage

219 A total of 71 pollen taxa were identified, among which *Pinus, Quercus*, Cyperaceae and *Typha*

220 were the most dominant taxa in the lower part (271–156 cm) of the core, and *Pinus*, *Quercus*,

221 Poaceae, Compositae, *Artemisia*, Chenopodiaceae and Cyperaceae were the most dominant taxa in

222 the upper part (156–0 cm) of the core. With respect to the fern spores, *Selaginella sinensis* and

223 Polypodiaceae were dominant; however, their content was low throughout the core. With the aid of

224 CONISS, the whole sequence was vertically divided into three zones, with zone 2 further

225 divided into subzones 2a, 2b, 2c and 2d (Figures 4 and 5).

226

4.3.1. Palynological zone 1 (271–156 cm)

228 The palynological zone 1 was characterized by abundant broadleaved trees pollen, dominated

229 by *Quercus* (mean 18.7%), *Betula*, *Alnus*, *Pterocarya*, Ulmaceae and Moraceae (Figure 4).

230 Percentages of conifer pollen were relatively low compared with other zones: *Pinus* ranges from

231 19.7% to 45.6% (mean 33.6%), and Taxodiaceae was present only occasionally. Compared to the

232 other zones, the proportions of non-arboreal pollen types, Compositae (mean 1.2%), *Artemisia*

233 (mean 4.2%), and Chenopodiaceae (mean 5.6%) were lowest in this zone, whereas the proportions

234 of Cyperaceae (mean 10.3%) and *Typha* (mean 11.2%) were highest in this zone. The palynological

235 concentrations were high, varying between 6050 and 237 grains/g (Figure 5).

236

4.3.2. Palynological zone 2 (156–30 cm)

238 Palynological zone 2 was divided into four subzones:

239 From depth of 156 to 128 cm (subzone 2a), the percentage of *Pinus* pollen reached its

240 maximum (mean 46.6%), whereas the percentage of broadleaved trees *Quercus* (16.1–9.5%, mean

241 14%), *Betula*, *Alnus*, *Pterocarya*, Ulmaceae, and Moraceae decreased to different degrees. The

242 proportions of non-arboreal pollen types, Compositae (mean 2.5%), *Artemisia* (mean 6.6%), and

243 Chenopodiaceae (mean 7.4%) were higher, whereas the percentages of Cyperaceae (mean 7.2%)

244 and *Typha* (mean 3.1%) declined sharply (Figure 4). Total pollen concentration were lower than in

245 zone 1, especially in the interval of 156–135 cm, where the value of total pollen concentrations (62–

246 1306 grains/g, mean 485 grains/g) was at its minimum in the core (Figure 5).

247 From depth of 128 to 63 cm (subzone 2b), *Pinus* (49.4–27.3%) and *Quercus* (18.1–7.9%, mean

248 13.5%) pollen level decreased to a low point, and the relative abundance of *Betula* slightly increased.

249 Occasionally, there were small amounts of *Pterocarya*, Ulmaceae, and Moraceae. Non-arboreal

250 pollen types, Compositae, *Artemisia*, and Chenopodiaceae continuously increased to averages of

251 3.5%, 6.7%, and 12%, respectively (Figure 4). Pollen concentration increased up to a high

252 abundance (mean 1260 grains/g) in this subzone (Figure 5).

253 From depth of 63 to 41 cm (subzone 2c), the percentage of *Pinus* pollen started to decrease

254 steadily, and the percentage of *Quercus* (17.4–11.8%, mean 14.8%), *Betula*, *Alnus*, *Pterocarya*, and

255 Ulmaceae pollen slightly increased. Similar to subzone 2b, this subzone had relatively high

256 quantities of non-arboreal pollen such as Compositae, *Artemisia*, and Chenopodiaceae (Figure 4).

257 Pollen concentrations varied between 456 and 1381 grains/g (Figure 5).

258 In contrast, subzone 2d (41–30 cm) was marked by a sudden decrease in the pollen of *Quercus*

259 (9.8%), and a steep increase in the pollen of *Pinus* (41.1%), even though the percentage of the non-

260 arboreal were the same as those of subzone 2c (Figure 4).

261

262 **4.3.3. Palynological zone 3 (30–0 cm)**

263 This zone was characterized by the transition from dominance by the pollen of arboreal taxa

264 to non-arboreal types. The percentage of *Pinus* and *Quercus* pollen decreased to the lowest level,

265 averaging approximately 19.7% and 5.5%, respectively. Poaceae, Compositae, *Artemisia*, and

266 Chenopodiaceae pollen increased, with average values of *Artemisia* and Chenopodiaceae reaching

267 up to 24.6% and 21.1%, respectively (Figure 4). The total pollen concentration declined to 188

268 grains/g in the lower part of the zone (30–19 cm) and then increased slightly (to approximately 621

269 grains/g) at the top (Figure 5).

270

271 **5. Discussion**

5.1. Key terrestrial palynomorphs proxies of environmental and climatic change

In sediment core CJ06–435, both *Pinus* and *Quercus* pollen were the predominant pollen types among the arboreal taxa. In order to understand the pollen provenance, the pollen records in the surface sediments of Laizhou Bay were studied (Yang et al., 2016), and the concentration and percentage data of main pollen species were presented on a regional map (Figure 6). Pollen results of surface sediments revealed that higher values of *Pinus* and *Quercus* are usually found in the eastern part of Laizhou Bay, and the lowest values of *Pinus* and *Quercus* occur in the nearshore area outside the mouth of the YR (Figure 6a and 6b). The distributions of *Pinus* and *Quercus* pollen in the surface sediments of Laizhou Bay are closely related to the distribution of the nearshore epicontinental vegetation. Except for the YRD, where there is swamp and cultivated land, the epicontinental region of the Laizhou Bay is surrounded by pine and oak forests. Among these, the land to the east of the Laizhou Bay (the Shandong Peninsula) belongs to the southern warm temperate zone and mainly supports a pine–oak forest dominated by *Pinus densiflora* and *Q. acutissima* (Wang et al., 1993). The land to the northeast of the Laizhou Bay (the Liaodong Peninsula) belongs to the southern temperate zone, and it mainly developing a conifer and broadleaved mixed forest dominated by *P. densiflora*, *Q. mongolica* and *Q. acutissima* (Li et al., 2007; Xu et al., 2010). The ubiquitous distribution of these plants on the adjacent terrain explains why *Pinus* and *Quercus* are the most common pollen taxa in Laizhou Bay, and why the highest concentration and percentage of *Pinus* and *Quercus* occurred in the eastern part of Laizhou Bay and the lowest values of *Pinus* and *Quercus* occurred on the nearshore area outside the mouth of the YR.

Previous studies have revealed that *Pinus* and *Quercus* were the most common components of the forests in northeast China (including the land areas surrounding the BS) during the Holocene. The variation of *Pinus* and *Quercus* contents were closely related to the change of temperature (Ren and Zhang, 1998; Yi et al., 2003; Li et al., 2004; Xu et al., 2014; Zhang et al., 2019). Ren and Zhang (1998) investigated pollen data from northeast China and found that *Quercus* and *Ulmus* were the dominant components of the forests between 10000 and 5000 a BP, while *Pinus* were much sparser, indicating warmer and drier summers in northeast China for the early to mid-Holocene. A high-resolution 1000-year pollen record from the Sanjiaowan Marr Lake in northeast China revealed that *Quercus* is an effective indicator for temperature reconstructions. Several notable cold periods, with

301 lower *Quercus* frequencies, occurred at approximately 1200 AD, 1410 AD, 1580 AD, 1770 AD and

302 1870 AD (Zhang et al., 2019). Another 5350-year pollen record from an annually laminated maar

303 lake in northeast China revealed a decrease of *Quercus* and increases of the *Pinus* component; this

304 indicates a cooling trend during the past 5350 years (Xu et al., 2014). Based on these results, we

305 conclude that the variation of *Pinus* and *Quercus* pollen of core CJ06-435 may be also related to

306 temperature change.

307 Herb pollen, especially Chenopodiaceae, also occupies an important position in core CJ06-435

308 (Figure 4). The spatial distribution of herb pollen in surface sediment of Laizhou Bay suggests that

309 a higher percentage and concentration occur in the nearshore area close to the YR estuary and the

310 southwestern part of Laizhou Bay, and a low percentage and concentration are found in the eastern

311 part of Laizhou Bay (Figure 6c and 6d). The YR is the main sediment source of the BS. The annual

312 mean sediment load of the YR was 1.08×10^9 tons before dam construction (Milliman and Meade,

313 1983), 70–90% of which was deposited and formed a huge delta complex (Zhou et al., 2016).

314 Natural vegetation in the modern YRD are dominated by wetland herbs, including Chenopodiaceae

315 and *Artemisia* (Jiang et al., 2013). Furthermore, under the combined action of the ocean and rivers,

316 alluvial plains and coast plains developed widely along the southern coast of Laizhou Bay. The

317 terrestrial vegetation types in these areas change from a bare intertidal zone to seepweed swamp to

318 reed swamp to cultivated land from the shoreline landward (Xu et al., 2010). Since the transportation

319 distance for herb pollen is normally very short, the pollen percentage and concentration in samples

320 close to the mouth of the YR and the southwestern part of Laizhou Bay are much higher than in

321 other samples (Figure 6c and 6d), indicating that herb pollen of Laizhou Bay is mainly derived from

322 the plant communities of the coastal wetlands.

323 It is worth noting that the composition of fossil pollen in sediment depends not only on the

324 composition of the vegetation from which the pollen originates but also on pollen dispersion,

325 deposition and preservation. *Pinus* pollen is a bisaccate grain, and has relatively high aerodynamic

326 and hydrodynamic characteristics meaning it can be transported efficiently by wind and water

327 (Sander, 2001; Montade et al., 2011). Previous studies revealed that smaller amount of *Pinus* pollen

328 are found nearshore, and larger amounts are found in the deep ocean (Mudie, 1982; Mudie and

329 McCarthy, 1994; Zheng et al., 2011; Dai et al., 2014; Luo et al., 2014; Dai and Weng, 2015). In

330 Laizhou Bay, although the concentration and percentage of *Pinus* pollen followed similar patterns

331   of distribution to broadleaved tree pollen (*Quercus*, *Betula* and *Carpinus*; Yang et al. 2016).

332   However, in the eastern part of Laizhou Bay, *Pinus* pollen increased in a northeasterly direction

333   away from the coast (Figure 6a). Hence, concerning *Pinus* pollen data, caution is required because

334   climate variation alone may not be responsible for the change of *Pinus* pollen in marine sediment.

335   Aerodynamic and hydrodynamic conditions may also influence the amounnt of *Pinus* pollen in

336   sediments.

337   In addition, because different pollen types are not equally well preserved (Havinga, 1967;

338   Cheddadi and Rossignol-Strick, 1995), bias originating from poor preservation should be eliminated

339   before using the net content of pollen grains to reconstruct paleovegetation. In this study, the pollen

340   concentration ranged from 62 to 6050 grains/g. Relatively low pollen concentrations were found in

341   the two sections (160–135 cm and 34–19 cm); this was largely correlated to high sand contents as

342   revealed by the lithology. Especially for the lower section (150–135 cm), the high portion of sand

343   content is consistent with a low pollen concentration and a high percentage of *Pinus* pollen. As the

344   *Pinus* pollen is more resistant to degradation, the variations of total pollen concentration as well as

345   a higher percentage of *Pinus* pollen in this section seem to be related to pollen preservation. But, as

346   shown in Figure 4, the highest percentage of *Pinus* pollen was recorded at a depth of 150–128 cm,

347   with a low value at 148 cm, which is not completely in accordance with the high sand content section

348   in the same core (160–135 cm). Similarly, for the upper section, a high sand content was recorded

349   at a depth of 34–19 cm. However, the percentage of *Pinus* pollen is low in this section, except for a

350   relatively high value at a depth of 23 cm. We thus suggest degradation is not a key point influencing

351   the concentration of pollen and spore in the study area.

352   Previous research suggests that the sedimentation mechanisms of pollen and spore in marine

353   water is similar to that of sediment with clay and fine silt grain size (Heusser, 1988). A recent

354   investigation on the surface sediment from the BS shows high pollen concentration in sediments

355   with a high proportion of fine particles such as clay and silty clay, while low pollen concentration

356   in sediments with a high proportion of coarser sand particles (Yang et al., 2019). Yang et al. (2019)

357   attributed the low pollen concentration in areas with a high sand content of the BS to the strong

358   hydrodynamic suspension and screening for sediments and pollen. We conclude that the low pollen

359   concentrations in the two sections (160–135 cm, and 34–19 cm), correlated with high sand content,

360   could be attributed to the hydrodynamic conditions rather than degradation.

5.2. Sedimentary records indicative of river channel shifts

The most important geological events in the northern China coast after 7000 a BP were the shift of YR channel and the formation of the YRD. The YR has been easily plugged and breached, and therefore its lower reaches migrated because of its huge sediment load. The shifting of the lower reaches of the YR led to the formation of a new delta superlobe (He et al., 2019). Based on a study of cheniers and historical documents, nine YRD superlobes have been proposed by Xue and Cheng (1989) and Xue (1993) on the western shore of the BS. Among these, superlobe 1 (7000–5000 a BP, He et al., 2019), superlobe 7 (11 AD–1048 AD, Xue, 1993), and superlobe 10 (1855 AD–present) are positioned near the core area in this study. The information about some of these superlobes formation are recorded in core CJ06-435.

As shown in Figure 8, herb percentage sudden change at 160 cm and 34 cm. Herb pollen in the sediment of Laizhou Bay is mainly derived from the coastal wetlands of the western BS. In 6000–7000 a BP and 1855 AD, the YR emptied into the BS after a natural course shift, forming two huge delta superlobes in the western part of the BS (Saito et al., 2000). Wetland plants are the most important vegetation type in the YRD (Jiang et al., 2013). The development of YRD wetland would change the amounts of herb pollen that was transported to the study site. In addition, the formation of YRD caused the coastline to move closer to the position of the CJ06-435 core. Since most herb plants are small in size, their pollen grains are unable to disperse broadly (Chen et al., 2019b). The migration of the coastline would change the availability of herb pollen to the study site, and hence lead to variations in the amount of pollen. Therefore, combined with the age data, we conclude that the abrupt change of herb pollen percentage at 160 cm and 34 cm in core CJ06-435 is related to the formation of the YRD superlobe 1 and superlobe 10.

Compared with the pollen percentage, the pollen concentration can be interpreted in different ways. Namely, the percentage of different types of pollen is relative, whereas the pollen concentration is absolute, and it can directly reflect the amounts of pollen that were transported to the study area (Luo et al., 2013). It is crucial that a correct interpretation of pollen data is based on a percentage diagram as well as concentration. In core CJ06-435, the concentrations of herbs—especially Chenopodiaceae and *Artemisia* (Figure 7f)—were higher at depths of 160–94 cm (6570–5000 a BP) and 34–0 cm (after 1855 AD), except for the two sections of 160–135 cm and 34–19

391   cm. As mentioned in section 5.1, the extremely low pollen concentration in the sections of 160–135

392   cm and 34–19 cm was closely linked with the coarser sandy sediment. Combined with the results

393   of pollen percentage and sediment grain size, we presumed that the higher herb pollen concentration

394   in the periods of 6570–5000 a BP (160–94 cm) and after 1855 AD (34–0 cm) reflects changes in

395   hydrographic conditions. Pollen data of surface sediments revealed that higher herb pollen

396   concentrations occur in the YR, and the value of these concentrations showed a decreasing trend

397   starting from the river mouth toward the ocean. The distribution pattern of surface pollen revealed

398   that the YR is a major carrier for most herbs taxa in the sediment of Laizhou Bay (Yang et al., 2016).

399   At the site of core CJ06-435, which is close to the mouth of the YR in Laizhou Bay, higher herb

400   pollen concentrations in the Holocene samples may indicate increased fluvial discharge.

401   Sediment grain size provides direct information on changes of the sediment source and the

402   sedimentary environment (Friedman and Sanders, 1978; Wu et al., 2015). The characteristics of

403   grain size can be expressed by the grain size distribution curve, and usually the mean or median

404   diameter is used (Xu, 1999). In this study, the value of mean grain size (Mz) showed that two major

405   grain size boundaries occur at depths of 34 and 19 cm, separating a middle sedimentary unit (34–19

406   cm) that contains coarser sediment from the lower and upper sedimentary units that contain finer

407   sediment (Figure 7d). The sand content of the upper, middle and lower layers was 11.2%, 33.6%,

408   and 9%, respectively (Figure 7a); the silt content of these layers was 69%, 58.6%, and 76.1%,

409   respectively (Figure 7b), and the clay content of these layers was 19.8%, 7.8%, and 14.8%,

410   respectively (Figure 7c). On the basis of ^{137}Cs chronology (Figure 3), we speculate that these

411   significant changes of grain size parameters at depths of 34 and 19 cm might represent a record of

412   the channel shifts of the YR in 1855 AD and 1976 AD, respectively.

413   The sediment of Laizhou Bay mainly comes from the YR and other small rivers located in

414   the southern part of Laizhou Bay (Zhang et al., 2017; Gao et al., 2018). Prior to 1855 AD, when the

415   YR entered the Yellow Sea, the sediment contribution to the BS from other small rivers was

416   relatively larger. The fine fraction suspension sediment that was derived from other small rivers

417   favors the hypothesis of fine sediment accumulation in core CJ06-435 during this period.

418   When the YR reentered the BS after 1855 AD, the dispersal of YR material contributed

419   substantially to the sedimentation of the BS. It was reported that more than 80% of the YR sediment

420   discharges into the BS during the summer period (Bi et al., 2011). Owing to the barrier effect of the

421 tidal shear front and the weak river flow, most of the river-delivered sediment is deposited on the

422 offshore delta within 15 km of the river mouth (Wang et al., 2007; Bi et al., 2010). Only a small part

423 of the fine clay fraction is transported by the coastal currents over long distances and deposited

424 across or along the shore in summer (Wu et al., 2015). During the winter (October to March) season,

425 the much stronger winter monsoon generates large waves, resulting in intensive sediment

426 resuspension in the coastal region owing to the enhanced bottom shear stress (Yang et al., 2011; Bi

427 et al., 2011). The resuspended sediment is transported southeastward along the coast of Laizhou Bay

428 by the monsoon-enhanced coastal currents passing through the location of the sediment core CJ06-

429 435. Therefore, after 1855 AD, the sediment of core CJ06-435 mainly included the fine fraction of

430 the suspended sediment dispersed from the YR mouth, the resuspended sediment from the coastal

431 area off the YR delta in the winter, and the locally resuspended sediment.

432   The accumulation of YR-suspended sediment during the summer season in Laizhou Bay was

433 closely associated with the sediment dispersion pattern off the active delta lobe (Xing et al., 2016).

434 The estuary of the YR, during most of the period 1855–1976 AD, was north of the modern YRD,

435 and suspended sediment from the YR was transported northeastward to Bohai Bay and the central

436 Bohai basin. The contribution of YR-suspended sediment to the sedimentation of core CJ06-435

437 was smaller and the resuspended sediment became a dominant material source. During the winter,

438 the large waves generated by the strong winds may result in intensive resuspension of the seabed

439 sediment and lead to part of the coarse sediment in the YR mouth and Laizhou Bay being transported

440 to the study area, which induces an evident increase in mean grain size and a decrease in the amount

441 of fine sediment. After 1976 AD, the lower channel of the YR shifted to the Qingshuigou course in

442 Laizhou Bay; the suspended sediments derived from the YR estuary were primarily driven

443 southward and southeastward along the coast, leading an increasing transportation of most of the

444 YR-suspended sediment into Laizhou Bay (Qiao et al., 2010). As a result, the dispersal of river-

445 laden sediment contributed substantially to the sedimentation of core CJ06-435, with a fine sediment

446 layer being formed in the upper part of the core.

447   The results inferred from our grain-size data on the migrations of the YR lower channel since

448 1855 AD and their effects on the sedimentary environments of the adjacent BS are in accordance

449 with the results of other studies from Laizhou Bay (Wu et al., 2015) and central BS (Hu et al., 2011).

450 Based on the records of sediment core collected from Laizhou Bay, Wu et al. (2015) found that when

451 the YR mouth approached the core location, the sediment became finer; otherwise, the active

452 resuspension resulted in the accumulation of coarser sediment owing to strong hydrodynamics. The

453 grain size results from the central mud areas of the BS also point to the conclusion that the sediment

454 supply from the YR to the central BS was cut off because of the shift of the YR terminal course

455 from the Diaokou source in outer Bohai Bay to the Qingshuigou course in Laizhou Bay in 1976;

456 hence, resuspended sediment became a primary source of sediment dispersal in the central BS. As

457 a result, there was a significant increase in the proportion of sand in surface sediment in the central

458 BS (Hu et al., 2011).

459 It is worth noting that the variation of grain size characteristics in the period of 6570–5000 a

460 BP is very similar to that after 1855 AD. As shown in Figure 7d, the shift of Mz in the period of

461 6570–5000 a BP also began with a significantly increased of Mz at 6570 a BP (160 cm) when the

462 YR flowed into the BS in northern Shangdong province. This similar variation of grain size in the

463 period of 6570–5000 a BP (superlobe 1) and after 1855 AD (superlobe 10) implies that a similar YR

464 channel shifting occurred during these two periods. However, further research is needed to reveal

465 how the deltaic and neritic sea sedimentary environment was impacted by the river system.

466

467 **5.3. Coastal salt marsh response to hydrological change**

468 Two high-amplitude salt marsh vegetation shifts are displayed in the herb pollen record during

469 6570–5000 a BP (superlobe 1) and after 1855 AD (superlobe 10), indicating rapid oscillations of

470 environmental conditions in the coastal area of BS. Within single intervals of the YR superlobe, a

471 recurrent and directional alternation of herb pollen taxa is observed in the following order: the shift

472 of herb pollen data began with an abrupt decrease of Cyperaceae pollen, followed by a steep increase

473 of Chenopodiaceae and *Artemisia* pollen (Figure 8b).

474 Cyperaceae, Chenopodiaceae, and *Artemisia* are the three plant families/genus that contain the

475 important representatives of coastal salt marsh plants (Lu et al., 2006). In the salt marsh of the

476 modern YRD, species composition of Cyperaceae, Chenopodiaceae, and *Artemisia* varies with

477 salinity and soil moisture. Plant families such as Cyperaceae are mainly composed of

478 hydrophytes and phreatophyte E*leocharis valleculosa*, *Cyperus rotundus*, *Scirpus planiculmis*, *S.*

479 *triqueter*, *S. yagara*, *S. juncoides*, and *Juncellus serotinus* (Pan and Xu, 2011). The presence of

480 Cyperaceae necessarily indicates lower saline conditions, since hydrophytes and phreatophyte

481   sedges typically colonize in the middle and upper part of the supralittoral zone, both sides along the

482   riverbank, the coast of the lake, and the interfluvial lowlands of the paleo-river. These areas are far

483   from the coastline, and the main type of soil is salinized soil with lower salinity (Zhang et al., 2009a;

484   Xu, 2011). Chenopodiaceae are mainly composed of halophyte *Suaeda glauca*, *S. salsa*, and

485   *Salicornia europaea*. *Artemisia* mainly consist of halophyte and xerophyte *Artemisia carvifolia*, *A.*

486   *capillaris*, and *A. annua* (Xing et al., 2003; Zhang et al., 2009b). In the modern YRD, halophytes

487   are distributed in the intertidal zone mudflat and the outside margin part of the supralittoral zone.

488   These areas are near the coastline, characterized by a high incidence of wave brakes and prolonged

489   inundation regimes, and the main type of soil is saline (Zhang et al., 2009b). Therefore, in salt marsh

490   plant communities, the variation in the amount of Cyperaceae, Chenopodiaceae, and *Artemisia* is

491   often thought to reflect environmental gradients controlled by the distance from the coast, local

492   topography, terrigenous material, and freshwater input (González and Dupont, 2009; Zhang et al.,

493   2009a). The pollen record from the BS could provide evidence of coastal salt marsh development

494   over decades to centuries of the response to environmental alternations during the period of

495   hydrological change.

496   In the studied sequence, the YR flowed into the BS toward the northern Shandong Province

497   after a course shift. The lower river was initially braided upon relocation, as characterized by

498   unchannelized river flow. At this initial stage, the river-derived sediment was largely accumulated

499   in the floodplain and/or among the antecedent rivers owing to the lack of channelization (Wu et al.,

500   2017), filling the coast of the lake, the interfluvial lowlands of the paleo-river, and the supralittoral

501   zone, etc. This caused the destruction of hydrophytes and phreatophyte sedges in these areas. This

502   process is indicated in our records by the significant decrease in the amount of Cyperaceae pollen

503   percentages for superlobe 1 and superlobe 10 (Figure 8b).

504   Eventually, natural channel adjustments resulted in the coalescence of multiple channels into

505   a single channel (Wu et al., 2017). A large amount of river-derived sediment was deposited at the

506   mouth of the YR, causing the progradation of the YRD. Because of the strong influence of the tides,

507   the intertidal zone in the YRD was originally bare beach. Along with the seaward expansion of the

508   newly formed beach, the influence of tides was weakening on the original bare beach wetland and

509   the salinity of the original beach wetland began to decrease (Zhang et al., 2007). Pioneer species of

510   salt marshes, e.g., *Suaeda glauca*, *S. salsa* and *Salicornia europaea* (Chenopodiaceae), first

511　colonized this original bare beach (Zhang et al., 2009a). The significant increase of Chenopodiaceae

512　in our pollen record (Figure 8b) is, therefore, interpreted as the development of the *S. glauca*

513　population.

514

515　**5.4. Palaeovegetation reconstruction and its climate significance**

516　　　Based on the age model, the record between 3000 a BP and 1855 AD of core CJ06-435 is

517　somewhat confused. Because the CSR was extremely low (about 0.005 cm/yr) during 3000 a BP to

518　1855 AD. As reported in recent studies, the CSR of cores from the tidal flat and neritic sea of the

519　south BS were in the range 0.02–0.13 cm/yr before 2000 a BP (in cores H9601, H9602, ZK228, and

520　ZK1, Figure 1; He et al., 2019), 0.04–0.06 cm/yr between 2000 a BP to 1855 AD (in cores ZK228,

521　HB-1, and GYDY, Figure 1; He et al., 2019), and 0.35–1.38 cm/yr since 1855 AD (Wu et al., 2015;

522　Qiao et al., 2017; Xu et al., 2018). Although core CJ06-435 is offshore compared to the other cores

523　(e.g. H9601, H9602, ZK228, HB-1, ZK1 and GYDY), and it should have a lower CSR compared to

524　those cores. But, the difference of CSR between CJ06-435 and those cores reach up to ten-fold. The

525　reasonable explanation is that there might be some deposition hiatus between 3000 a BP and 1855

526　AD of core CJ06-435. The calculated CSR in the upper layer (since 1855 AD, as calculated to 0.17–

527　0.48 cm/yr) and the lower layer (3000–8500 a BP, as calculated to 0.016–0.057 cm/yr) of core CJ06-

528　435 are comparable to the nearby records by He et al. (2019) and Xu et al. (2018). Therefore, we

529　just focused on the vegetation successions and climate change between 8500 and 3000 a BP, and

530　only gave a cautious discussion for the chronology uncertain interval in this study.

531　　　During the period from 8500 to 6500 a BP (palynological zone 1, 271–156 cm), the

532　palynofloral assemblages are mainly composed of the pollen of broadleaved trees, such as *Quercus,*

533　*Betula*, *Alnus*, and Ulmaceae, combined with the pollen of hydrophytes and phreatophyte

534　Cyperaceae and *Typha*; of these, the pollen of *Quercus* and *Typha* are predominant (Figures 4 and

535　5). In contrast, the pollen of halophytic and xerophytic herbs and conifer trees is scarce. The pollen

536　assemblages encountered herein indicated that the vegetation of the BS land area consisted mainly

537　of oak-rich temperate broadleaf deciduous forest, with some conifer trees on the uplands, and

538　freshwater lakes and marshes dominating the coastal area, under the influence of a markedly warmer

539　and wetter climate than the present. The highest values of AP pollen concentration (Figure 5),

540　reflecting a dense vegetation cover, also represent warm conditions during this period. The pollen

541 data are comparable to that found from previous palynological studies carried out in north China

542 (e.g., Yi et al., 2003; Ren, 2007; Chen and Wang, 2012; Li et al., 2019) and northeast China (e.g.,

543 Ren and Beug, 2002; Li et al., 2011; Stebich et al., 2015), from which a warm, wet climate

544 corresponding to the Holocene Optimum was inferred. Under the influence of the Holocene

545 Optimum, the forest cover evidently increased in north and northeast China (Ren, 2007). In the YR

546 drainage area and Shandong Peninsula, the broadleaved deciduous forest thrived, accompanied by

547 the presence of monsoonal evergreen forest and the abrupt decrease in the herbaceous taxa and

548 conifers (Yi et al., 2003; Chen and Wang, 2012; Li et al., 2019).

549 During the period from 6500–5900 a BP (palynological zone 2a, 156–128 cm), a climatic

550 cooling period is identified by an increase of conifers, *Pinus*, combined with an abrupt reduction of

551 broadleaved trees (*Quercus*, *Betula*, *Alnus*, *Pterocarya*, Ulmaceae, and Moraceae). Halophytic and

552 xerophytic herbs taxa such as Compositae, *Artemisia*, and Chenopodiaceae also increase, while

553 Cyperaceae and aquatic herbs *Typha* obviously decreased. The climate shifted from warm, wet to

554 cool, and dry may have caused the reduction of broadleaved deciduous forests, the expansion of

555 conifer forests, and the gradually disappearance of freshwater lakes and marshes that had spread

556 over the coastal area of BS. This result is in good agreement with previous studies. A pollen record

557 from Shandong Peninsula revealed that *Quercus* content decreased, and herbs increased quickly

558 following the Holocene Optimum, indicating a potential climate deterioration (Chen and Wang,

559 2012). A pollen record from Lake Bayanchagan in southern Inner Mongolia also showed that

560 deciduous trees declined, conifers reached their maximum values, whilst steppe vegetation remained

561 relatively high during 6500–5100 a BP, indicating cold and dry climate conditions (Jiang et al.,

562 2006). It is worth noting that, a vast delta complex began to build up in the western part of the BS

563 after 6570 a BP, which resulted in the increase of land area and development of the YR delta wetland.

564 It can be concluded that the expansion of salt marsh during this period may be partly related to the

565 formation of the YR delta complex.

566 During the period from 5900–3500 a BP (palynological zone 2b, 128–63 cm), climate cooling

567 and drying is observed by a reduction of broadleaved trees such as *Quercus*, *Pterocarya*, Ulmaceae

568 and Moraceae, and a rising frequency of halophytic and xerophytic herbs (*Artemisia* and

569 Chenopodiaceae) (Figures 4 and 5). The cool, dry conditions probably cause the contraction of

570 broadleaved forest and the expansion of halophytic and xerophytic herbs, which is similar to the

571 findings of a study by Jiang et al. (2006). Based on the quantitative climatic reconstruction from

572 pollen and algal data for Lake Bayanchagan, Jiang et al. (2006) found that broadleaved trees, such

573 as *Betula*, *Corylus*, *Ostryopsis* and *Ulmus* further declined, whereas the amount of steppe vegetation

574 increased. The reconstruction of mean annual temperature and total annual precipitation dropped to

575 their minimum values during 5100–2600 a BP.

576   Between 3500 and 3000 a BP (63–56 cm), a warm climatic phase occurred, as suggested by an

577 increase in the amount of pollen from broadleaved trees (*Quercus*, *Betula*, *Alnus*, *Pterocarya*, and

578 Ulmaceae), with low frequencies of conifer pollen (*Pinus*). Moreover, halophytic and xerophytic

579 herb pollen, including Compositae, *Artemisia*, and Chenopodiaceae, were still present at a high

580 frequency (Figures 4 and 5). Accordingly, the assemblages reveal that a warm, dry climate probably

581 developed during this period.

582   From 3000 a BP to 1855 AD (56–30 cm), as mentioned in the first paragraph of this section,

583 the CSR was extremely low during the period from 3000 a BP to 1855 AD (56–30 cm). We suggest

584 that there might be some deposition hiatus and only tentatively discuss this section of the pollen

585 record. This section begins with a relatively high percentage of broadleaved trees (*Quercus*, *Betula*,

586 *Alnus*, *Pterocarya*, and Ulmaceae) and low frequencies of conifer pollen (*Pinus*) (56-41 cm); this is

587 consistent with the previous stage (3500–3000 a BP, 63-56 cm). Afterward, there is a dramatic

588 decrease in the occurrence of *Quercus*, quickly followed by a sudden increase in *Pinus* (41–30 cm,

589 Figures 4 and 5). These pollen data suggest that the climate was warm during the latter part of this

590 period (56–41 cm, 3000 a BP–?), following the climate condition of previous stage (63–56 cm,

591 3500–3000 a BP). In the earlier part of this period (41–30 cm, ?–1855 AD), the sudden increase in

592 *Pinus* and major reductions of *Quercus* are likely signs of human impacts on the natural vegatation,

593 including deforestation and cultivation. Park and Kim (2015) interpreted the decrease in the

594 percentage of *Quercus* and increase of *Pinus* in the late Holocene as marking the development of

595 secondary vegetation under anthropogenic influence. Based on two boreholes palynological from

596 the YRD, Yi et al. (2003) found a sudden reduction of *Quercus*, followed by a marked increase of

597 *Pinus* after 1300 a BP. Their research considered that this typical lag between the two taxa may

598 indicate that, after the clearance of the local broadleaved deciduous forests, the vegetation was

599 replaced by a secondary pine forest.

600   After 1855 AD (palynological zone 3, 30–0 cm), a significant decline in broadleaved trees

601 (*Quercus*) and conifers (*Pinus*) pollen, as well as an increase in the frequency of herbs (Poaceae,

602 Compositae, *Artemisia*, and Chenopodiaceae) pollen may reflect the further strengthening of human

603 disturbance on the vegetation and the expansion of intensive agricultural cultivation into forests of

604 the BS coastal area. Moreover, after 1855 AD, the present YR began returning to the BS, and

605 forming a vast area of floodplain and estuarine wetland on the southwest coast of the BS (Saito et

606 al., 2000; Jiang et al., 2013). The variation of herb pollen may be partly related to the development

607 of the modern YRD wetland.

608

609 **5.5. Holocene temperature variations in north China and possible driving mechanisms**

610   Many previous studies of north and northeast China have used the *Quercus* pollen percentage

611 to infer regional temperature variation (Ren and Zhang, 1998; Yi et al., 2003; Li et al., 2004; Xu et

612 al., 2014; Zhang et al., 2019). The *Quercus* pollen percentage from CJ06-435 core is consistent with

613 previous studies, which also provide a regional air temperature reference. As shown in Figure 9d,

614 the percentage of *Quercus* pollen in CJ06-435 core indicates a warm early Holocene from 8500 to

615 6500 a BP, a cool mid-Holocene from 6500 to 3500 a BP, and then a relatively warm late Holocene.

616 These climate changes were also apparent in the change of *Quercus*/*Pinus* (Q/P) ratio. The average

617 Q/P ratio was approximately 0.57 between 8500 and 6500 a BP, and changed to 0.33 between 6500

618 and 3500 a BP, and then gradually increased (Figure 9c).

619   The pollen-based record of temperature evolution from core CJ06-435 are broadly in-phase

620 with published high-resolution sea surface temperature record from core YS01 (Figure 9e) of the

621 Yellow Sea, suggesting at least a local pattern of temperature variations during the Holocene. To

622 investigate whether the temperature pattern was local characteristics of the BS and Yellow Sea area,

623 or whether it was rather a regional patterns of East Asia as a whole, the pollen records of core CJ06-

624 435 were compared with recently-published and relatively well-dated sequences from north China,

625 northwest China, and the Tibetan Plateau (see Figure 9a for site locations), including the

626 sedimentary pollen-based temperature record from the Narenxia Peat within the Kanas Lake,

627 Northwest China (Figure 9f; Feng et al., 2017); U^K_{37} inferred temperature record at Lake Qinghai

628 (Figure 9g; Hou et al., 2016); and lacustrine sedimentary pollen-based quantitative temperature

629 record (the mean annual temperature) from Lake Bayanchagan in Inner Mongolia in north China

630 (Figure 9h; Jiang et al., 2006). All three records indicate that the temperature was high between

631 8500 and 6000 a BP, low between 6000 and 4000–3000 a BP, and averagely high after 4000–3000

632 a BP (Figure 9f–h), this is consistent with the basic change pattern of our pollen-based temperature

633 variation (Figure 9c and 9d). The comparison of the five records demonstrates that the CJ06-435

634 core *Quercus* pollen percentage record is, at a minimum, of regional significance.

635 Insolation has been widely accepted as an important factor in Holocene climate variation. The

636 covariation of Northern Hemisphere extratropical (30 ° to 90 ° N) temperature and local summer

637 insolation on an orbital scale, and the long-term decrease of summer insolation make the especially

638 pronounced cooling of the Northern Hemisphere extra-tropics during the Holocene (Marcott et al.,

639 2013) appear reasonable. However, the general pattern of temperature variation revealed by our

640 study is not entirely consistent with local mean annual insolation forcing (Figure 9b). Our results

641 indicated a cold mid-Holocene from 6500 to 3500 a BP and a relatively warm late Holocene. This

642 temperature characterization of a cool mid-Holocene and a relatively warm late Holocene is also

643 seen in many proxy records in the East Asia (Thompson et al., 1997; Jiang et al., 2006; Hou et al.,

644 2016; Wu et al., 2016; Feng et al., 2017; Jia et al., 2019). The cooler mid-Holocene seen in the East

645 Asia, could not solely be explained by the gradually decreasing summer insolation during the

646 Holocene but might be related to other forcings.

647 We compared the pollen-based temperature record of core CJ06-435 (Figure 9c and 9d) with

648 the frequency of El Niño events reconstructed from the Botryococcene concentration in the El Junco

649 Lake sediment (Figure 9i; Zhang et al., 2014) and the ENSO variability reconstructed from $\delta^{18}O$

650 values of individual planktonic foraminifera retrieved from deep-sea sediments (Figure 9j; Koutavas

651 and Joanides, 2012). As shown in Figure 9, lower temperature periods in the mid-Holocene tend to

652 occur during a period of low El Niño activity, a relatively high temperature period in late Holocene

653 tend to occur during a period of high El Niño activity, which indicates that there may be some link

654 between the temperature of BS and Yellow Sea area and the ENSO system. Modern research

655 suggests that ENSO can influence the evolution of temperature behavior, over interannual to multi-

656 decadal time ranges (Hoerling et al., 2008; Triacca et al., 2014). In East Asia, many studies have

657 indicated that the East Asian winter monsoon and the ENSO are tightly coupled (Zhou et al., 2007;

658 Cheung et al., 2012; An et al., 2017). Generally, the strength of winter monsoon and East Asia

659 troughs weakens in an El Niño year, and the weakening could cause the observed winter half-year

660 warming (Xu et al., 2005). On centennial/millennial time scales, using pollen data from Lake Moon

in the central part of the Great Khingan Mountain Range, Wu et al. (2019) recently connected increased El Niño frequency with the decrease of winter monsoon activity in the East Asia, and the warming winter temperature in the Great Khingan Mountain Range since the mid-Holocene. Feng et al. (2017) founded that warm-phased ENSO was teleconnected with weakening of the Siberian High, and that the weakening was a cause of the observed winter half-year warming in southern Siberia. Likewise, the results of this study, indicating more or less synchronicity of the climate change in north China and ENSO activity, provide a possible linkage between the climate of north China and oceanic forcing during the mid-late Holocene.

In addition, radiative forcing by greenhouse gases (GHGs) rose 0.5 W/m^2 during the mid-late Holocene (Marcott et al., 2013), which would be expected to yield 1°C warming at Kinderlinskaya Cave in the southern Ural Mountains from 7000 a BP to the pre-industrial (Baker et al., 2017). Recently, both winter insolation and GHG forcing have been proposed as the major driving factors for winter warming during the Holocene in the Siberian Arctic (Meyer et al., 2015) and the southern Ural Mountains (Baker et al., 2017). Similarly, summer warming in central Asia during the mid-late Holocene, recorded by the alpine peat α-cellulose $\delta^{13}C$ record from the Altai Mountains (Rao et al., 2019), has been proposed to be mainly driven by the enhanced GHG forcing and increasing human activities. Rao et al. (2020) suggested that GHG forcing was the dominant driver of the summer and winter warming trends since ~5000 a BP. The effects of GHG forcing are global. Hence, we suggest that enhanced GHG forcing may be an important driver for mid-late Holocene temperature variations of East Asia.

In summary, the temperature characterizations of a cool mid-Holocene and a relatively warm late-Holocene revealed by the East Asia records could be linked with the change of insolation, ENSO activity and GHG forcing. The cooler mid-Holocene may be related to a combination of the decreasing summer insolation, weak El Niño activity, and relatively lower GHG radiative forcing during this interval. Along with strengthened ENSO activity and enhanced GHG forcing in the late Holocene, there was increased temperature.

6. Conclusions

Through the palynological and grain size reconstruction of coastal area vegetation and environment in core CJ06-435, we were able to identify specific responses of plant communities to

climatic (temperature, precipitation), hydrological, and anthropogenic impacts. Our data elucidate the pattern and mechanisms driving coastal salt marsh succession at decade-to-century timescales. Two intervals of expanded salt marsh vegetation correspond to the formation of YR delta superlobes, indicating that soil development and salinity gradients are the main factors determining the vegetation dynamics of coastal wetland. Our pollen-based temperature index revealed a warm early Holocene (8500–6500 a BP), a subsequent cool stage between 6500 and 3500 a BP, and a slightly warming episode after 3500 a BP. The reliability of the record, especially the cooler mid-Holocene, is further supported by several other temperature records from East Asia. We suggest that changes in insolation, ENSO activity and GHG forcing could have played an important role in the temperature evolution at the East Asia.

Code/Data availability

The co-authors declare that all data included in this study are available upon request by contact with the corresponding author (Email: *jinxiachen@fio.org.cn*).

Author contribution

Chen Jinxia wrote the manuscript; Shi Xuefa and Liu Yanguang revised the manuscript; Qiao Shuqing provided many constructive suggestions for the manuscript; Yang Shixiong provided the pollen data of surface sediment; Li Jianyong use pollen data of core CJ06-435 as base for quantitative climate reconstruction; Yan Shijuan, Lv Huahua, Li Xiaoyan and Li Chaoxin provided financial support for the collection of samples and obtained samples.

Competing interests

The authors declare that they have no conflict of interest.

Acknowledgements

References

An, S.I., Kim, H.J., Park, W., Schneider, B.: Impact of ENSO on East Asian winter monsoon during interglacial periods: Effect of orbital forcing, Clim. Dynam., 49, 3209–3219, 2017.

Bao, R., Alonso, A., Delgado, C., Pagés, J.L.: Identification of the main driving mechanisms in the evolution of a small coastal wetland (Traba, Galicia, NW Spain) since its origin 5700 cal yr BP, Palaeogeogr. Palaeoclimatol. Palaeoecol., 247, 296–312, 2007.

Baker, J.L., Lachniet, M.S., Chervyatsova, O., Asmerom, Y., Polyak, V.: Holocene warming in western continental Eurasia driven by glacial retreat and greenhouse forcing, Nat. Geosci., https://doi.org/10.1038/NGEO2953, 2017.

Bi, N.S., Yang, Z.S., Wang, H.J., Hu, B.Q., Ji, Y.J.: Sediment dispersion pattern off the present Huanghe (Yellow River) subdelta and its dynamic mechanism during normal river discharge period, Estuar. Coast. Shelf. S., 86, 352–362, 2010.

Bi, N.S., Yang, Z.S., Wang, H.J., Fan, D.J., Sun, X.X., Lei, K.: Seasonal variation of suspended-sediment transport through the southern Bohai Strait, Estuar. Coast. Shelf. S., 93, 239–247, 2011.

Cheddadi, R., Rossignol-Strick, M.: Improved preservation of organic matter and pollen in Eastern Mediterranean sapropels, Paleoceanography, 10 (2), 301-309, 1995.

Chen, J.X., Nan, Q.Y., Li, T.G., Sun, R.T., Sun, H.J., Lu, J.: Variations in the East Asian winter monsoon from 3500 to 1300 cal. yr BP in northern China and their possible societal impacts, J. Asian. Earth. Sci., https://doi.org/10.1016/j.jseaes.2019.103912, 2019a.

Chen, J.X., Li, T.G., Nan, Q.Y., Shi, X.F., Liu, Y.G., Jiang, B., Zou, J.J., Selvaraj, K., Li, D.L., Li, C.S.: Mid-late Holocene rainfall variation in Taiwan: A high-resolution multiproxy record unravels the dual influence of the Asian monsoon and ENSO, Palaeogeogr. Palaeoclimatol. Palaeoecol., 516, 139–151, 2019b.

Chen, W., Wang, W.M.: Middle-Late Holocene vegetation history and environment changes revealed by pollen analysis of a core at Qingdao of Shandong Province, East China, Quat. Int., 254, 68–72, 2012.

Cheung, H.N., Zhou, W., Mok, H.Y., Wu, M.C.: Relationship between Ural-Siberian blocking and the East Asian winter monsoon in relation to the Arctic Oscillation and the El Niño-Southern Oscillation, J. Climate., 25(12), 4242–4257, 2012.

Cohen, M.C.L., Lara, R.J., Smith, C.B., Angélica, R.S., Dias, B.S., Pequeno, T.: Wetland dynamics of Marajó Island, northern Brazil, during the last 1000 years, Catena, 76(1), 70–77, 2008.

Cohen, M.C.L., Pessenda, L.C.R., Behling, H., Rossetti, D.d.F., França, M.C., Guimarães, J.T.F., Friaes, Y., Smith, C.B.: Holocene palaeoenvironmental history of the Amazonian mangrove belt, Quat. Sci. Rev., 55, 50–58, 2012.

Cui, B.S., Yang, Q.C., Yang, Z.F., Zhang, K.J.: Evaluating the ecological performance of wetland restoration in the Yellow River Delta, China, Ecol. Eng., 35, 1090–1103, 2009.

762 Dai, L., Weng, C.Y., Lu, J., Mao, L.M.: Pollen quantitative distribution in marine and fluvial surface
763   sediments from the northern South China Sea: new insights into pollen transportation and deposition
764   mechanisms, Quat. Int., 325, 136–149, 2014.

765 Dai, L., Weng, C.Y.: Marine palynological record for tropical climate variations since the late last glacial
766   maximum in the northern South China Sea, Deep-sea. Res. Pt. II., 122, 153–162, 2015.

767 Engelhart, S.E., Horton, B.P., Roberts, D.H., Bryant, C.L., Corbett, D.R.: Mangrove pollen of Indonesia
768   and its suitability as a sea-level indicator, Mar. Geol., 242, 65–81, 2007.

769 Faegri, K., Iversen, J.: Textbook of Pollen Analysis, Alden Press, London, 370, 1992.

770 Feng, Z.D., Sun, A.Z., Abdusalih, N., Ran, M., Kurban, A., Lan, B., Zhang, D.L., Yang, Y.P.: Vegetation
771   changes and associated climatic changes in the southern Altai Mountains within China during the
772   Holocene, Holocene, 27(5), 683–693, 2017.

773 França, M.C., Francisquini, M.I., Cohen, M.C.L., Pessenda, L.C.R., Rossetti, D.F., Guimarães, J.T.F.,
774   Smith, C.B.: The last mangroves of Marajó Island–Eastern Amazon: Impact of climate and/or
775   relative sea-level changes, Rev. Palaeobot. Palyno., 187, 50–65, 2012.

776 França, M.C., Alves, I.C.C., Castro, D.F., Cohen, M.C.L., Rossetti, D.F., Pessenda, L.C.R., Lorente, F.L.,
777   Fontes, N.A., Junior, A.Á.B., Giannini, P.C.F., Francisquini, M.I.: A multi-proxy evidence for the
778   transition from estuarine mangroves to deltaic freshwater marshes, Southeastern Brazil, due to
779   climatic and sea-level changes during the late Holocene, Catena, 128, 155–166, 2015.

780 Friedman, G.M., Sanders, J.E.: Principles of sedimentology, John Wiley and Sons, Inc, 1–792, 1978.

781 Gao, M.S., Guo, F., Hou, G.H., Qiu, J.D., Kong, X.H., Liu, S., Huang, X.Y., Zhuang, H.H.: The evolution
782   of sedimentary environment since late Pleistocene in Laizhou Bay, Bohai Sea, Geol. Chin., 45(1),
783   59–68, 2018. (in Chinese with English abstract)

784 Giraldo-Giraldo, M.J., Velásquez-Ruiz, C.A., Pardo-Trujillo, A.: Late-Holocene pollen-based
785   paleoenvironmental reconstruction of the El Triunfo wetland, Los Nevados National Park (Central
786   Cordillera of Colombia), Holocene, 28(2), 183–194, 2018.

787 González, C., Dupont, L.M.: Tropical salt marsh succession as sea-level indicator during Heinrich events,
788   Quat. Sci. Rev., 28, 939–946, 2009.

789 Grimm, E.C.: CONISS: a Fortran 77 program for stratigraphically constrained cluster analysis by the
790   method of incremental sum of squares. Comput. Geosci., 13, 13–35, 1987.

791 Gu, Y.H., Xiu, R.C.: On the current and storm flow in the Bohai Sea and their role in transporting
792   deposited silt of the Yellow River, J. Oceanogr. Huanghai & Bohai Seas., 14(1), 1–6, 1996.

793 Hao, T., Liu, X.J., Ogg, J., Liang, Z., Xiang, R., Zhang, X.D., Zhang, D.H., Zhang, C., Liu, Q.L., Li,
794   X.G.: Intensified episodes of East Asian Winter Monsoon during the middle through late Holocene
795   driven by North Atlantic cooling events: High-resolution lignin records from the South Yellow Sea,
796   China, Earth. Planet. Sci. Lett., 479, 144–155, 2017.

797 Havinga, A.J.: Palynology and pollen preservation, Rev. Palaeobot. Palyno., 2, 81–98, 1967.

798 He, L., Xue, C.T., Ye, S.Y., Amorosi, A., Yuan, H.M., Yang, S.X., Laws, E.A.: New evidence on the
799   spatial-temporal distribution of superlobes in the Yellow River Delta Complex, Quat. Sci. Rev., 214,
800   117–138, 2019.

801 Hemavathi, S., Manjula, R., Ponmani, N.: Numerical Modelling and Experimental Investigation on the
802   Effect of Wave Attenuation Due to Coastal Vegetation, Proceedings of the Fourth International
803   Conference in Ocean Engineering (ICOE2018), 23, 99–110, 2019.

804 Hendy, I.L., Minckley, T.A., Whitlock, C.: Eastern tropical Pacific vegetation response to rapid climate
805   change and sea level rise: A new pollen record from the Gulf of Tehuantepec, southern Mexico,

806   Quat. Sci. Rev., 145, 152–160, 2016.

807   Heusser, L.E.: Pollen distribution in marine sediments on the continental margin off northern California.
808   Mar. Geol., 80, 131–147, 1988.

809   Hoerling, M., Kumar, A., Eischeid, J., Jha, B.: What is causing the variability in global mean land
810   temperature?, Geophys. Res. Lett., 35, L23712, 2008.

811   Hou, X.Y.: Vegetation Atlas of China, Science Press, 1–280, 2001. (in Chinese)

812   Hou, J.Z., Huang, Y.S., Zhao, J.T., Liu, Z.H., Colman, S., An, Z.S.: Large Holocene summer temperature
813   oscillations and impact on the peopling of the northeastern Tibetan Plateau, Geophys. Res. Lett., 43,
814   1323–1330, 2016.

815   Hu, L.M., Guo, Z.G., Shi, X.F., Qin, Y.W., Lei, K., Zhang, G.: Temporal trends of aliphatic and
816   polyaromatic hydrocarbons in the Bohai Sea, China: Evidence from the sedimentary record, Org.
817   Geochem., 42, 1181–1193, 2011.

818   Huang, D.J., Su, J.L., Backhaus, J.O.: Modelling the seasonal thermal stratification and baroclinic
819   circulation in the Bohai Sea, Cont. Shelf. Res., 19, 1485–1505, 1999.

820   Jia, Y.H., Li, D.W., Yu, M., Zhao, X.C., Xiang, R., Li, G.X., Zhang, H.L., Zhao, M.X.: High- and low-
821   latitude forcing on the south Yellow Sea surface water temperature variations during the Holocene,
822   Global. Planet. Change., 182, 103025, 2019.

823   Jiang, W.Y., Guo, Z.T., Sun, X.J., Wu, H.B., Chu, G.Q., Yuan, B.Y., Hatte, C., Guiot, J.: Reconstruction
824   of climate and vegetation changes of Lake Bayanchagan (Inner Mongolia): Holocene variability of
825   the east Asian monsoon, Quat. Res., 65, 411–420, 2006.

826   Jiang, D.J., Fu, X.F., Wang, K.: Vegetation dynamics and their response to freshwater inflow and climate
827   variables in the Yellow River Delta, China, Quat. Int., 304, 75–84, 2013.

828   Kirchner, G., Ehlers, H.: Sediment Geochronology in Changing Coastal Environments: Potentials and
829   Limitations of the ^{137}Cs and [210]Pb Methods, J. Coast. Res., 14, 483–492, 1998.

830   Koutavas, A., Joanides, S.: El Niño-Southern Oscillation extrema in the Holocene and Last Glacial
831   Maximum, Paleoceanography, https://doi.org/10.1029/2012PA002378, 2012.

832   Li, C.Y., Yan, L.Q., Han, T.X.: Research on composition of wetland vegetation in Shandong, Shandong
833   Forest Sci. Tech., 4, 27–29, 2007. (in Chinese with English abstract)

834   Li, X.Q., Zhou, J., Shen, J., Weng, C.Y., Zhao, H.L., Sun, Q.L.: Vegetation history and climatic variations
835   during the last 14 ka BP inferred from a pollen record at Daihai Lake, north-central China, Rev.
836   Palaeobot. Palyno., 132, 195–205, 2004.

837   Li, C.H., Wu, Y.H., Hou, X.H.: Holocene vegetation and climate in Northeast China revealed from Jingbo
838   Lake sediment, Quat. Int., 229, 67–73, 2011.

839   Li, G.G., Hu, B.Q., Bi, J.Q., Song, Z.L., Bu, R.Y., Li, J.M.: Stratigraphic evolution of the Huanghe Delta
840   (Bohai Sea) since the Late Quaternary and its paleoenvironmental implications: evidence from core
841   ZK1, Acta. Sedimentol. Sin., 31 (6), 1050–1058, 2013. (in Chinese with English abstract)

842   Li, M.Y., Zhang, S.R., Xu, Q.H., Xiao, J., Wen, R.L.: Spatial patterns of vegetation and climate in the
843   North China Plain during the Last Glacial Maximum and Holocene climatic optimum, Sci. China.
844   Earth. Sci., 62 (8), 1279–1287, 2019.

845   Liu, J., Saito, Y., Wang, H., Zhou, L., Yang, Z.: Stratigraphic development during the Late Pleistocene
846   and Holocene offshore of the Yellow River delta, Bohai Sea, J. Asian. Earth. Sci., 36, 318–331,
847   2009a.

848   Liu, W.Z., Zhang, Q.F., Liu, G.H.: Seed banks of a river–reservoir wetland system and their implications
849   for vegetation development, Aquat. Bot., 90, 7–12, 2009b.

850   Liu, S., Feng, A., Du, J., Xia, D., Li, P., Xue, Z., Hu, W., Yu, X.: Evolution of the buried channel systems
851   under the modern Yellow River delta since the last glacial maximum, Quat. Int., 349, 327–338, 2014.
852   Liu, D.Y., Li, X., Emeis, K.C., Wang, Y.J., Richard, P.: Distribution and sources of organic matter in
853   surface sediments of Bohai Sea near the Yellow River Estuary, China, Estuar. Coast. Shelf. S., 165,
854   128–136, 2015.
855   Lu, J.J., He, W.S., Tong, C.F., Wang, W.: Wetland Ecology. Higher Education Press, Beijing, 2006.
856   Luo, C.X., Chen, M.H., Xiang, R., Liu, J.G., Zhang, L.L., Lu, J., Yang, M.X.: Characteristics of modern
857   pollen distribution in surface sediment samples for the northern South China Sea from three
858   transects, Quat. Int., 286, 148–158, 2013.
859   Luo, C.X., Chen, M.H., Xiang, R., Liu, J.G., Zhang, L.L., Lu, J., Yang, M.X.: Modern pollen distribution
860   in marine sediments from the northern part of the South China Sea, Mar. Micropaleontol., 108, 41–
861   56, 2014.
862   Marcott, S.A., Shakun, J.D., Clark, P.U., Mix, A.C.: A reconstruction of regional and global temperature
863   for the past 11,300 years, Science, 339, 1198–1201, 2013.
864   Meyer, H., Opel, T., Laepple, T., Dereviagin, A.Y., Hoffmann, K., Werner, M.: Long-term winter
865   warming trend in the Siberian Arctic during the mid- to late Holocene, Nat. Geosci., https://doi.org/
866   10.1038/NGEO2349, 2015.
867   Milliman, J.D., Meade, R.H.: World-wide delivery of river sediment to oceans, J. Geol., 91, 1–21, 1983.
868   Milliman, J.D., Qin, Y.S., Ren, M.E., Saito, Y.: Man's influence on the erosion and transport of sediment
869   by Asian rivers: the Yellow River (Huanghe) example, J. Geol., 95, 751–762, 1987.
870   Montade, V., Nebout, N.C., Kissel, C., Mulsow, S.: Pollen distribution in marine surface sediments from
871   Chilean Patagonia, Mar. Geol., 282, 161–168, 2011.
872   Mudie, P.J.: Pollen distribution in recent marine sediments, Eastern Canada, Can. J. Earth Sci., 19, 729–
873   747, 1982.
874   Mudie, P.J., Mc Carthy, F.M.G.: Pollen transport processes in the western North Atlantic: evidence from
875   cross margin and north–south transects, Mar. Geol., 118, 79–105, 1994.
876   Neumann, F.H., Scott, L., Bousman, C.B., As, L.V.: A Holocene sequence of vegetation change at Lake
877   Eteza, coastal KwaZulu-Natal, South Africa, Rev. Palaeobot. Palyno., 162, 39–53, 2010.
878   Pan, Y., Xu, J.W.: Studies on Resource and Flora of Aquatic Vascular Plants in Wetland of Yellow River
879   Delta, J. Anhui. Agr. Sci., 39(3), 1642–1644, 2011. (in Chinese with English abstract)
880   Palinkas, C.M., Nittrouer, C.A.: Modern sediment accumulation on the Po shelf, Adriatic Sea, Cont.
881   Shelf. Res., 27, 489–505, 2007.
882   Park, J., Kim, M.: Pollen-inferred late Holocene agricultural developments in the vicinity of Woljeong-
883   ri, southwestern Korea, Quat. Int., 384, 13–21, 2015.
884   Pessenda, L.C.R., Vidotto, E., Oliveira, P.E.D., Jr, A.A.B., Cohen, M.C.L., Rossetti, D.d.F., Ricardi-
885   Branco, F., Bendassolli, J.A.: Late Quaternary vegetation and coastal environmental changes at Ilha
886   do Cardoso mangrove, southeastern Brazil, Palaeogeogr. Palaeoclimatol. Palaeoecol., 363–364, 57–
887   68, 2012.
888   Qiao, F.L., Gan, Z.J., Sun, X.P.: Regional oceanography of China seas-physical oceanography, China.
889   Ocean. Press., 2012.
890   Qiao, S.Q., Shi, X.F., Zhu, A.M., Liu, Y.G., Bi N.S., Fang, X.S., Yang, G.: Distribution and transport of
891   suspended sediments off the Yellow River (Huanghe) mouth and the nearby Bohai Sea, Estuar. Coast.
892   Shelf. S., 86, 337–344, 2010.
893   Qiao, S.Q., Shi, X.F., Wang, G.Q., Zhou, L., Hu, B.Q., Hu, L.M., Yang, G., Liu, Y.G., Yao, Z.Q., Liu,

894   S.F.: Sediment accumulation and budget in the Bohai Sea, Yellow Sea and East China Sea, Mar.
895   Geol., 390, 270–281, 2017.

896 Rao, Z.G., Huang, C., Xie, L.H., Shi, F.X., Zhao, Y., Cao, J.T., Gou, X.H., Chen, J.H., Chen, F.H.: Long-
897   term summer warming trend during the Holocene in central Asia indicated by alpine peat α-cellulose
898   δ^{13}C record, Quat. Sci. Rev., 203, 56–67, 2019.

899 Rao, Z.G., Shi, F.X., Li, Y.X., Huang, C., Zhang, X.Z., Yang, W., Liu, L.D., Zhang, X.P., Wu, Y.: Long-
900   term winter/summer warming trends during the Holocene revealed by α-cellulose δ^{18}O/δ^{13}C records
901   from an alpine peat core from central Asia. Quat. Sci. Rev., 232, 106217, 2020.

902 Ren, G.Y., Zhang, L.S.: A preliminary mapped summary of Holocene pollen data for northeast China,
903   Quat. Sci. Rev., 17, 669–688, 1998.

904 Ren, G.Y., Beug, H.J.: Mapping Holocene pollen data and vegetation of China, Quat. Sci. Rev., 21, 1395–
905   1422, 2002.

906 Saito, Y., Wei, H.L., Zhou, Y.Q., Nishimura, A., Sato, Y., Yokota, S.: Delta progradation and chenier
907   formation in the Huanghe (Yellow River) delta, China, J. Asian. Earth. Sci., 18, 489–497, 2000.

908 Sander, V.D.K.: Pollen distribution in marine sediments from the south-eastern Indonesian waters,
909   Palaeogeogr. Palaeoclimatol. Palaeoecol., 171, 341–361, 2001.

910 Serrano, O., Lovelock, C.E., Atwood, T.B., Macreadie, P.I., Canto, R., Phinn, S., Arias-Ortiz, A., Bai, L.,
911   Baldock, J., Bedulli, C., et al.: Australian vegetated coastal ecosystems as global hotspots for climate
912   change mitigation, Nat. Commun., https://doi.org/10.1038/s41467–019–12176–8, 2019.

913 Spivak, A.C., Sanderman, J., Bowen, J.L., Canuel, E.A., Hopkinson, C.S.: Global-change controls on
914   soil-carbon accumulation and loss in coastal vegetated ecosystems, Nat. Geosci., 12, 685–692, 2019.

915 Stebich, M., Rehfeld, K., Schlütz, F., Tarasov, P.E., Liu, J.Q., Mingram, J.: Holocene vegetation and
916   climate dynamics of NE China based on the pollen record from Sihailongwan Maar Lake, Quat. Sci.
917   Rev., 124, 275–289, 2015.

918 Stuiver, M., Reimer, P.J., Reimer, R.W.: CALIB 7.1 [WWW program, http://calib.org], 2019.

919 Thompson, L.G., Yao, T.D., Davis, M.E., Henderson, K.A., Mosley-Thompson, E., Lin, P.N., Beer, J.,
920   Synal, H.A., Cole-Dai, J., Bolzan, J.F.: Tropical climate instability: the last glacial cycle from a
921   Qinghai-Tibetan ice core, Science, 276, 1821–1825, 1997.

922 Triacca, U., Pasini, A., Attanasio, A., Giovannelli, A., Lippi, M.: Clarifying the Roles of Greenhouse
923   Gases and ENSO in Recent Global Warming through Their Prediction Performance, J. Clim., 27,
924   7903–7910, 2014.

925 Wang, K.F. and others: Spore-pollen and algal assemblages in the sediments of the Bohai Sea and
926   palaeoenvironments, Geological Publishing House, Beijing, 1993.

927 Wang, H., Yang, Z., Li, Y., Guo, Z., Sun, X., Wang, Y.: Dispersal pattern of suspended sediment in the
928   shear frontal zone off the Huanghe (Yellow River) mouth, Cont. Shelf. Res., 27, 854–871, 2007.

929 Wang, H.J., Wang, A.M., Bi, N.S., Zeng, X.M., Xiao, H.H.: Seasonal distribution of suspended sediment
930   in the Bohai Sea, China, Cont. Shelf. Res., 90, 17–32, 2014.

931 Woodroffe, S.A., Long, A.J., Milne, G.A., Bryant, C.L., Thomas, A.L.: New constraints on late Holocene
932   eustatic sea-level changes from Mahe, Seychelles, Quat. Sci. Rev., 115, 1–16, 2015.

933 Wu, X., Bi, N.S., Kanai, Y., Saito, Y., Zhang, Y., Yang, Z.S., Fan, D.J., Wang, H.J.: Sedimentary records
934   off the modern Huanghe (Yellow River) delta and their response to deltaic river channel shifts over
935   the last 200 years, J. Asian. Earth. Sci., 108, 68–80, 2015.

936 Wu, P., Xiao, X., Tao, S., Yang, Z., Zhang, H., Li, L., Zhao, M.: Biomarker evidence for changes in
937   terrestrial organic matter input into the Yellow Sea mud area during the Holocene, Sci. China. Earth.

938   Sci., 59, 1216–1224, 2016.

939   Wu, X., Bi, N.S., Xu, J.P., Nittrouer, J.A., Yang, Z.S., Saito, Y., Wang, H.J.: Stepwise morphological

940   evolution of the active Yellow River (Huanghe) delta lobe (1976–2013): Dominant roles of riverine

941   discharge and sediment grain size, Geomorphology, https://doi.org/10.1016/

942   j.geomorph.2017.04.042, 2017.

943   Wu, J., Liu, Q., Cui, Q. Y., Xu, D. K., Wang, L., Shen, C. M., Chu, G.Q., Liu, J.Q.: Shrinkage of East

944   Asia winter monsoon associated with increased ENSO events since the mid-Holocene, J. Geophys.

945   Res., 124, 3839–3848, 2019.

946   Xing, S.Y., Xi, J.B., Zhang, J.F., Song, Y.M., Ma, B.Y.: The basic characteristics and the main types of

947   vegetation in the Yellow River delta region, J. Northeast. Forest. Univ., 31(6), 85–86, 2003. (in

948   Chinese)

949   Xing, G.P., Wang, H.J., Yang, Z.S., Bi, N.S.: Spatial and temporal variation in erosion and accumulation

950   of the subaqueous Yellow River delta (1976-2004), J. Coast. Res., 74, 32–47, 2016.

951   Xu, J.X.: Grain-size characteristics of suspended sediment in the Yellow River, China, Catena, 38, 243–

952   263, 1999.

953   Xu, W.C., Ma, J.s., Wang, W.: A review of studys on the influence of ENSO events on the climate in

954   China, Sci. Meteorol. Sin., 25(2), 212–220, 2005.

955   Xu, J.W.: Research on Diversity of Aquatic Vascular Plants in Wetland of Yellow River Delta,

956   Heilongjiang. Agr. Sci., 1, 36–38, 2011. (in Chinese with English abstract)

957   Xu, D.K., Lu, H.Y., Chu, G.Q., Wu, N.Q., Shen, C.M., Wang, C., Mao, L.M.: 500-year climate cycles

958   stacking of recent centennial warming documented in an East Asian pollen record, Sci. Rep-UK., 4,

959   3611, 2014.

960   Xu, Y.P., Zhou, S.Z., Hu, L.M., Wang, Y.H., Xiao, W.J.: Different controls on sedimentary organic carbon

961   in the Bohai Sea: River mouth relocation, turbidity and eutrophication. J. Marine. Syst., 180, 1–8,

962   2018.

963   Xu, Z.J., Zhang, X.L., Zhang, Z.H., Zhang, W.: Analysis of the biodiversity characters of coastal wetlands

964   in southern Laizhou Bay, Ecol. Env. Sci., 19(2), 367–372, 2010. (in Chinese with English abstract)

965   Xue, C., Cheng, G.D., Zhou, Y.Q.: Relationship between Late Pleistocene and Early Holocene terrestrial

966   deposits and sea level changes in Yellow River Delta area. Mar. Geol. Quat. Geol., 8 (2), 63–73,

967   1988. (in Chinese with English abstract)

968   Xue, C.T., Cheng, G.D.: Shelly ridges in west coast of Bohai Sea and Holocene Yellow River Delta

969   system. In: Yang, Z.G., Lin, H.M. (Eds.), Quaternary Processes and Events in China Offshore and

970   Onshore Areas, China. Ocean. Press., 1989. (in Chinese with English abstract)

971   Xue, C.T.: Historical changes in the Yellow River delta, China, Mar. Geol., 113, 321–329, 1993.

972   Xue, C.T., Zhu, X.H., Lin, H.M.: Holocene sedimentary sequence, foraminifera and ostracoda in west

973   coastal lowland of Bohai Sea, China, Quat. Sci. Rev., 14, 521–530, 1995.

974   Yang, Z.S., Ji, Y.J., Bi, N.S., Lei, K., Wang, H.J.: Sediment transport off the Huanghe (Yellow River)

975   delta and in the adjacent Bohai Sea in winter and seasonal comparison, Estuar. Coast. Shelf. S., 93,

976   173–181, 2011.

977   Yang, S.X., Li, J., Mao, L.M., Liu, K., Gao, M.S., Ye, S.Y., Yi, S., Zhou, L.Y., Wang, F.F.: Assessing

978   pollen distribution patterns and provenance based on palynological investigation on surface

979   sediments from Laizhou Bay, China: an aid to palaeoecological interpretation, Palaeogeogr.

980   Palaeoclimatol. Palaeoecol., 457, 209–220, 2016.

981   Yang, S.X., Song, B., Ye, S.Y., Laws, E.A., He, L., Li, J., Chen, J.X., Zhao, G.M., Zhao, J.T., Mei, X.,

Behling, H.: Large-scale pollen distribution in marine surface sediments from the Bohai Sea, China: Insights into pollen provenance, transport, deposition, and coastal-shelf paleoenvironment, Prog. Oceanog., 178, 102183, 2019.

Yi, S., Saito, Y., Oshima, H., Zhou, Y.Q., Wei, H.L.: Holocene environmental history inferred from pollen assemblages in the Huanghe (Yellow River) delta, China: climatic change and human impact, Quat. Sci. Rev., 22, 609–628, 2003.

Zhang, G.S., Wang, R.Q., Song, B.M.: Plant community succession in modern Yellow River Delta, China, J. Zhejiang Univ. Sci., 8(8), 540–548, 2007.

Zhang, X.L., Ye, S.Y., Yin, P., Chen, D.J.: Characters and successions of natural wetland vegetation in Yellow River Delta, Ecol. Env. Sci., 18(1), 292–298, 2009a. (in Chinese with English abstract)

Zhang, X.L., Ye, S.Y., Yin, P., Yuan, H.M.: Flora characteristics of vascular plants of coastal wetlands in Yellow River Delta, Ecol. Env. Sci., 18(2), 600–607, 2009b. (in Chinese with English abstract)

Zhang, Z.H., Leduc, G., Sachs, J.P.: El Niño evolution during the Holocene revealed by a biomarker rain gauge in the Galápagos Islands, Earth. Planet. Sci. Lett., 404, 420–434, 2014.

Zhang, P., Hu, R.J., Zhu, L.H., Wang, P., Yin, D.X., Zhang, L.J.: Distributions and contamination assessment of heavy metals in the surface sediments of western Laizhou Bay: Implications for the sources and influencing factors, Mar. Pollut. Bull., https://doi.org/10.1016/j.marpolbul.2017.03.046, 2017.

Zhang, H.X., Zhang, M.L., Xu, T.P., Tang, J.: Numerical Investigations of Tsunami Run-Up and Flow Structure on Coastal Vegetated Beaches, Water, https://doi.org/10.3390/w10121776, 2018.

Zhang, J.Y., Li, J., Yan, Y., Li, J.J., Wan, X.Q.: A 1000-year record of centennial-scale cyclical vegetation change from Maar Lake Sanjiaolongwan in northeastern China, J. Asian. Earth. Sci., 176, 315–324, 2019.

Zheng, Z., Yang, S.X., Deng, Y., Huang, K.Y., Wei, J.H., Berne, S., Suc, J.P.: Pollen record of the past 60 ka BP in the Middle Okinawa Trough: Terrestrial provenance and reconstruction of the paleoenvironment, Palaeogeogr. Palaeoclimatol. Palaeoecol., 307, 285–300, 2011.

Zhou, L.Y., Liu, J., Saito, Y., Gao, M.S., Diao, S.B., Qiu, J.D., Pei, S.F.: Modern sediment characteristics and accumulation rates from the delta front to prodelta of the Yellow River (Huanghe), Geo-Mar. Lett., 36, 247–258, 2016.

Zhou, W., Wang, X., Zhou, T.J., Li, C., Chan, J.C.L.: Interdecadal variability of the relationship between the East Asian winter monsoon and ENSO, Meteorol. Atmos. Phys., 98, 283–293, 2007.

Zhou, Z., Bian, C., Wang, C., Jiang, W., Bi, R.: Quantitative assessment on multiple timescale features and dynamics of sea surface suspended sediment concentration using remote sensing data, J. Geophys. Res-Oceans., 122, 8739–8752, 2017.

Table captions

Table 1

AMS radiocarbon dates from core CJ06-435 and one tie points corresponding to the deepest onset of

[137]Cs in environmental samples at measurable levels; for calibration in years before present (a BP) 0 =

1950 AD.

Core depth (cm)	Materials	Radiocarbon date (a)	Age error (a)	Calibrated age (1σ) (a BP)	Mean calibrated age (a BP)	Laboratory
25	[137]Cs	–	–	–	–4	NIGLAS
7	Mixed benthic foraminifera	3020	30	2854-3039	2951	Beta
13	Mixed benthic foraminifera	2990	30	2817-2997	2913	Beta
17	Mixed benthic foraminifera	3060	30	2908-3102	3003	WHOI
59	Mixed benthic foraminifera	3340	30	3270-3485	3359	Beta
69	Mixed benthic foraminifera	3590	25	3563-3725	3656	WHOI
87	Mixed benthic foraminifera	4450	30	4695-4878	4801	Beta
119	Mixed benthic foraminifera	5200	30	5604-5770	5706	WHOI
129	Mixed benthic foraminifera	4520	30	4812-4965	4894	Beta
161	Mixed benthic foraminifera	6020	30	6501-6667	6592	WHOI
183	Mixed benthic foraminifera	6340	35	6886-7081	6981	WHOI

Figure caption

Figure 1: Geographic map of the Bohai Sea, with locations of core CJ06-435 (red circle) and other sites referred to in this study (purple circles). Cores references: H9601 and H9602 (Saito et al., 2000), ZK1 (Li et al., 2013), ZK228 (Xue et al.,1988), HB-1 (Liu et al., 2009a), GYDY (Liu et al., 2014).

Figure 2: Vegetation map around the Bohai Sea and the ocean current in the Bohai Sea during the summer (a) and winter (b) (YSWC: Yellow Sea Warm Current; SBSCC: Southern Bohai Sea Coastal Current; LNCC: Liaonan Coastal Current; LBCC: Lubei Coastal Current, modified from Qiao et al., 2010; the vegetation dataset was provided by the Environmental and Ecological Science Data Center for West China, National Natural Science Foundation of China [http://westdc.westgis.ac.cn] and is based on the Vegetation Atlas of China, 1:1000,000; Hou, 2001).

Figure 3: Lithology, grain size, color reflectance a*, magnetic susceptibility, and activity profiles for ^{137}Cs and ^{210}Pb of core CJ06-435.

Figure 4: Percentage diagram of the principal pollen taxa from core CJ06-435. Pollen zonation is based on CONISS results.

Figure 5: Concentration diagram of the principal pollen taxa from core CJ06-435.

Figure 6: Spatial distribution of modern pollen percentage (black solid circle, %) and concentration (red open circle, grains/g) in Laizhou Bay, Bohai Sea (modified from Yang et al., 2016).

Figure 7: (a-f) Vertical profiles of grain-size parameters and halophytic and xerophytic herb (Chenopodiaceae and *Artemisia*) pollen percentage and concentration of core CJ06-435 (Mz – mean grain size). (g) The location of Yellow River superlobe 1 (Lijin superlobe) and superlobe 10 (Modern superlobe) (modified after Xue, 1993).

Figure 8: (a) Correlating proxy to paleo-superlobe variation of the YR, from top to bottom: percentage of Cyperaceae, Chenopodiaceae, and *Artemisia* pollen; concentration of Chenopodiaceae, *Artemisia*, and Cyperaceae pollen; sand percentage. (b) Detailed pollen and grain size profiles representing salt marsh species (Cyperaceae, Chenopodiaceae, *Artemisia*) relative abundances and hydrodynamic change during the formation of Yellow River superlobe 1 and 10. Pollen percentage of Cyperaceae, Chenopodiaceae and *Artemisia* from core CJ06-435 indicating the directional alternation of salt marshes along the Bohai Sea, ①— Unchannelized river flow characterized the onset of Yellow River channel shift, caused a large amount of river–derived sediment accumulation in the floodplain and destroyed the sedges in the coastal depression; ②

1091 —Along with the formation of a new channel, lateral migration of the lower channel stopped, and

1092 new intertidal mudflat was formed. Pioneer species (Chenopodiaceae, *Artemisia*) first colonize

1093 bare zones of lower and middle marsh areas.

1094

1095

1096 **Figure 9:** Comparison of relevant Holocene temperature records with solar irradiance and ENSO

1097 proxy records derived from the equatorial Pacific. (a) Locations of the sites where the Holocene

1098 temperature records are derived. The schematic large-scale diagram modified from Hao et al.

1099 (2017). In the diagram, the purple area is Tibetan Plateau, the yellow area is Chinese Loess Plateau,

1100 and red circle refer to the corresponding study sites. (b) Summer (mean of June) insolation

1101 irradiance for the Northern Hemisphere (40°N). (c,d) *Quercus*/*Pinus* (Q/P) rate and *Quercus* pollen

1102 percentage records from core CJ06-435, bold-blue and bold-red lines are the five-point running

1103 average. As introduced in part 5.4 "Palaeovegetation reconstruction and its climate significance",

1104 there might be some deposition hiatus between 3000 a BP and 1855 AD. So, Q/P rate and *Quercus*

1105 pollen percentage records during 3000 a BP and 1855 AD is for reference only. (e) $U^{K'}_{37}$ SST record

1106 from YS01 core in the south Yellow Sea (Jia et al., 2019). (f) Pollen-based mean annual temperature

1107 (MAT) record from Narenxia Peat in the southern Altai (Feng et al., 2017). (g) U^{K}_{37} inferred

1108 temperature record at Lake Qinghai (Hou et al., 2016). (h) Pollen-based mean annual temperature

1109 record from Lake Bayanchagan in Inner Mongolia, North China (Jiang et al., 2006). (i)

1110 Botryococcene concentrations in the El Junco sediment, a proxy for frequency of El Niño events

1111 (Zhang et al., 2014). (j) Variance of $\delta^{18}O$ values of individual planktonic foraminifera (*G. ruber*) in

1112 sediment core V21–30 from the Galápagos region, a proxy for ENSO variance (Koutavas and

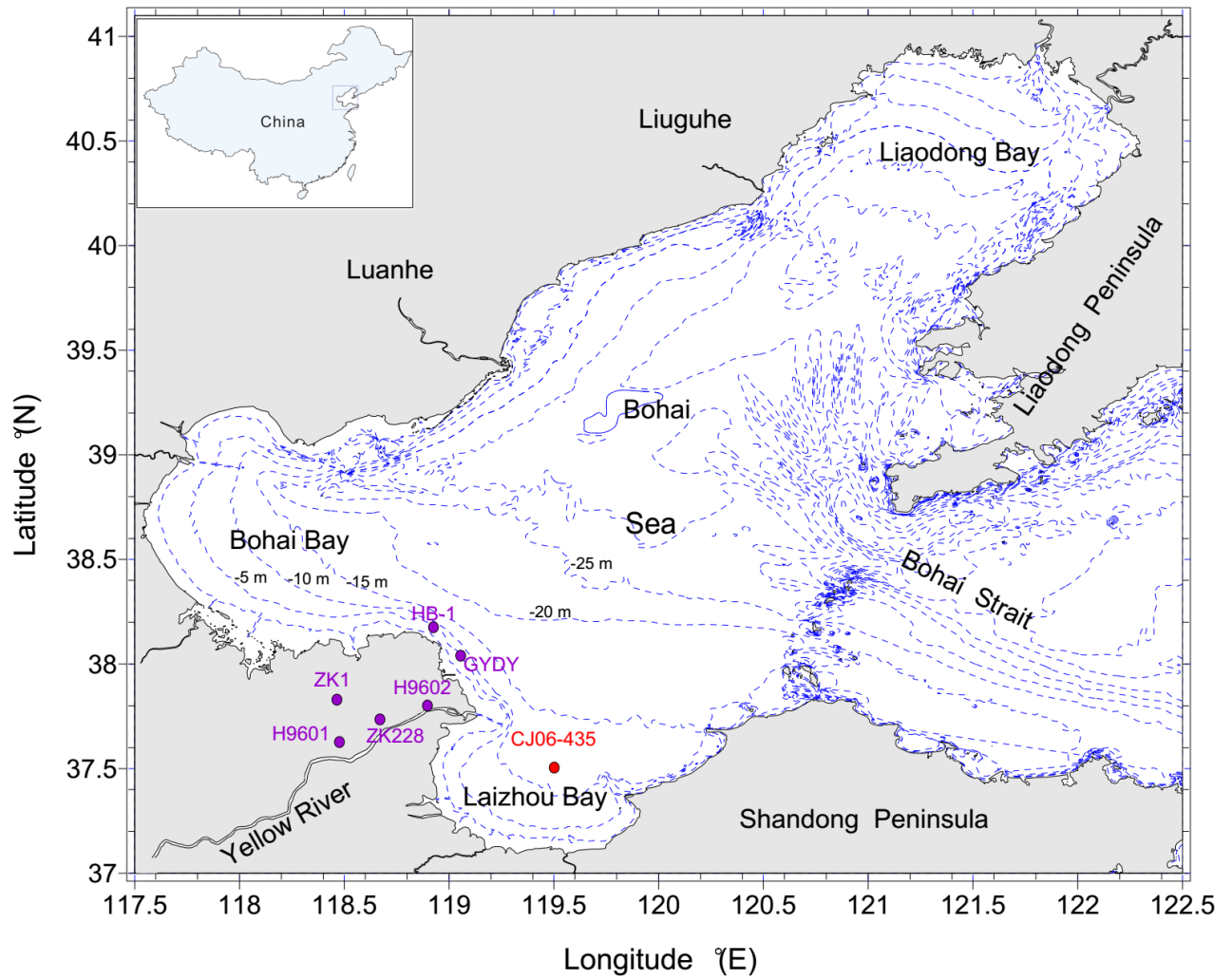1113 Joanides, 2012).

1114

1115
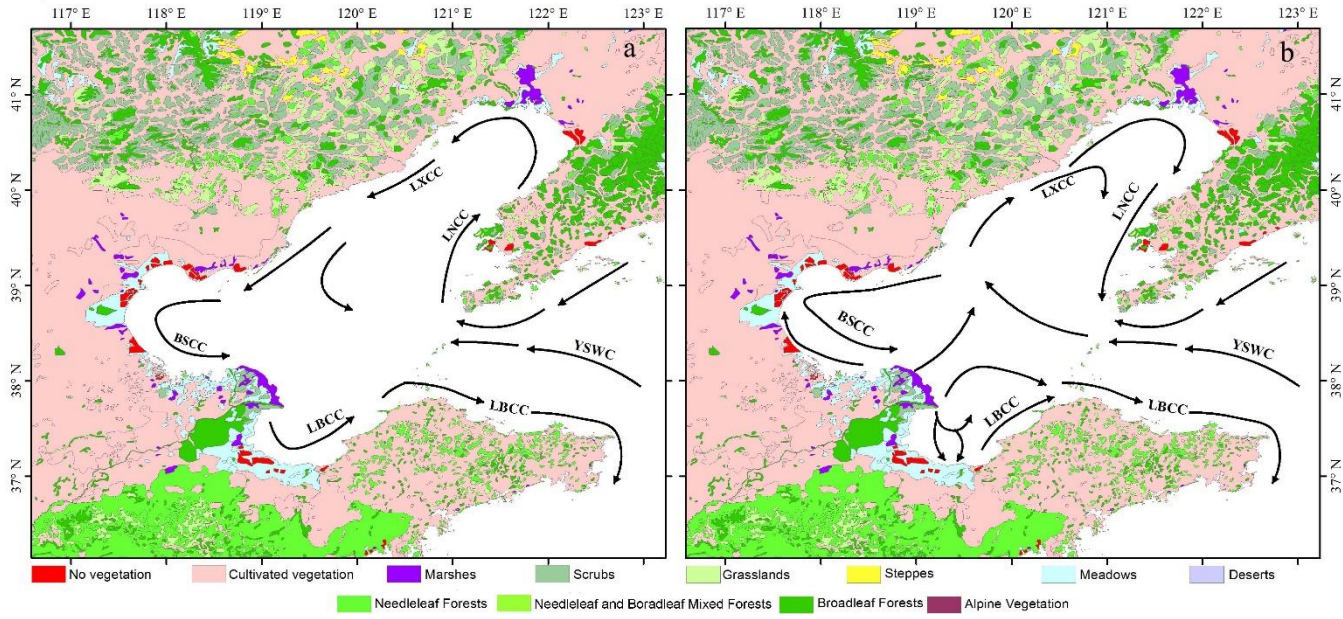
1116

1117

1118

1119

1120

1121

1122

1123

Figure 1

1124

1125

1126

1127

1128
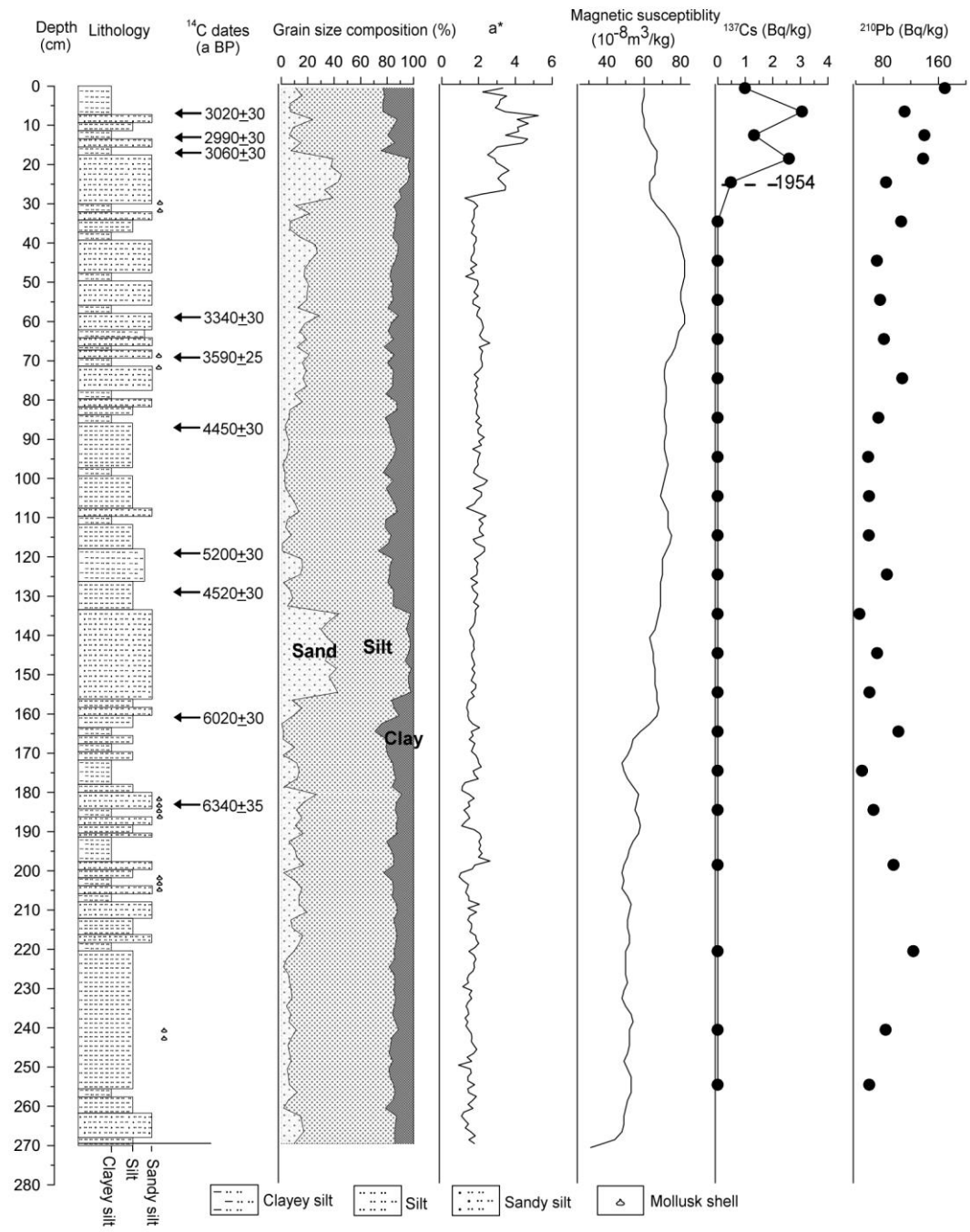
Figure 2

1129

1130

1131

Figure 3

1132

Figure 4

1133

Figure 5

1134
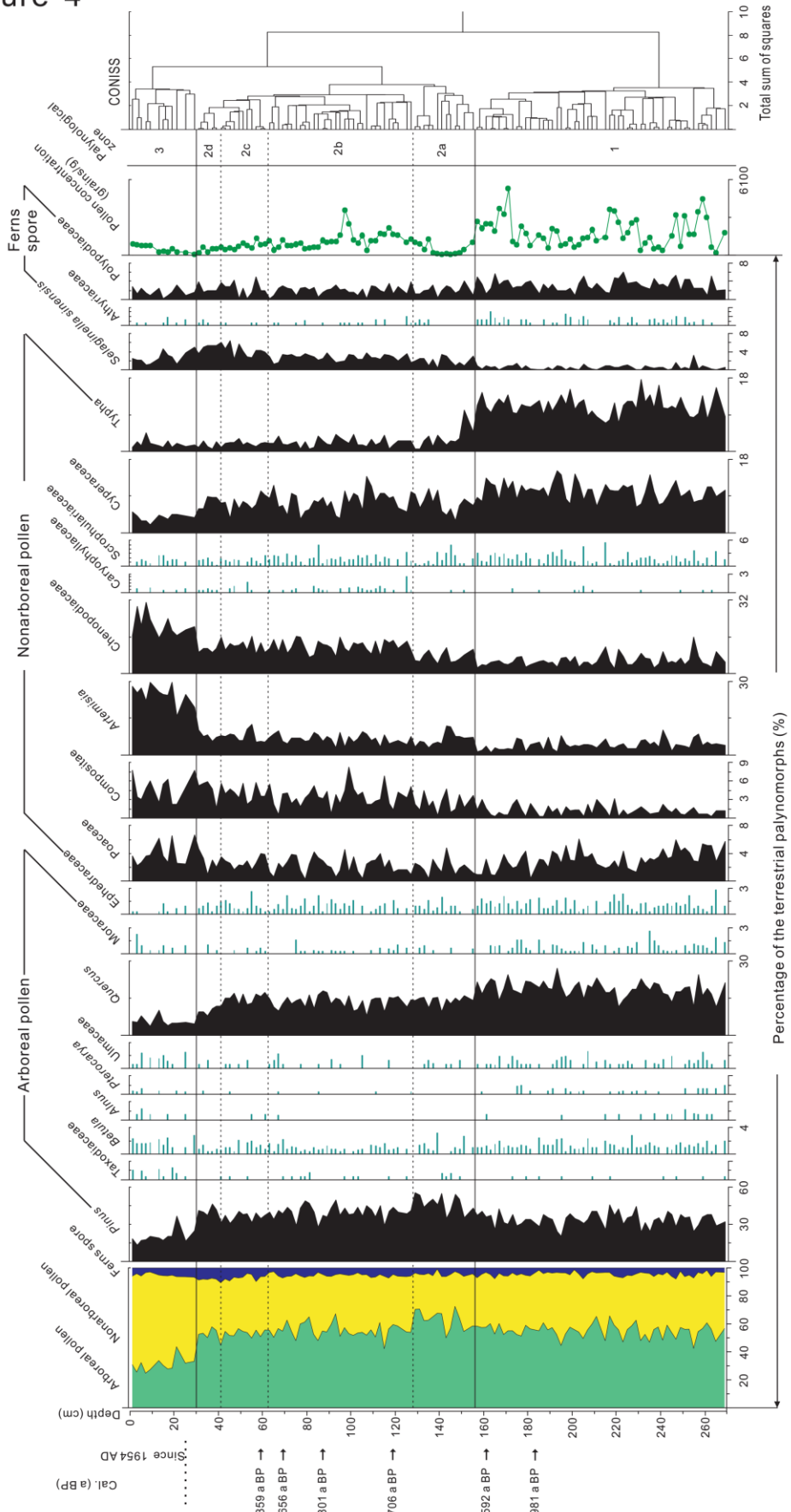
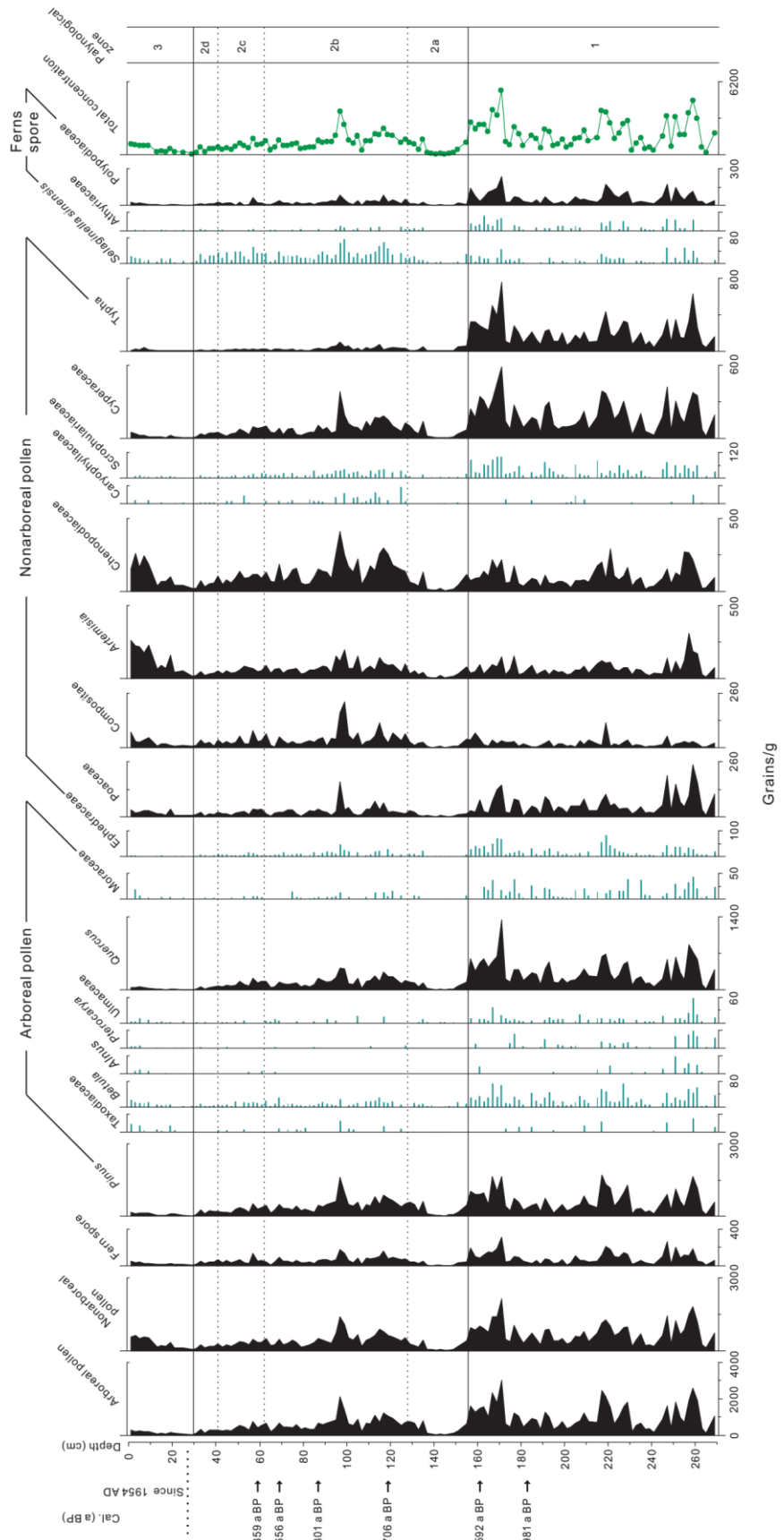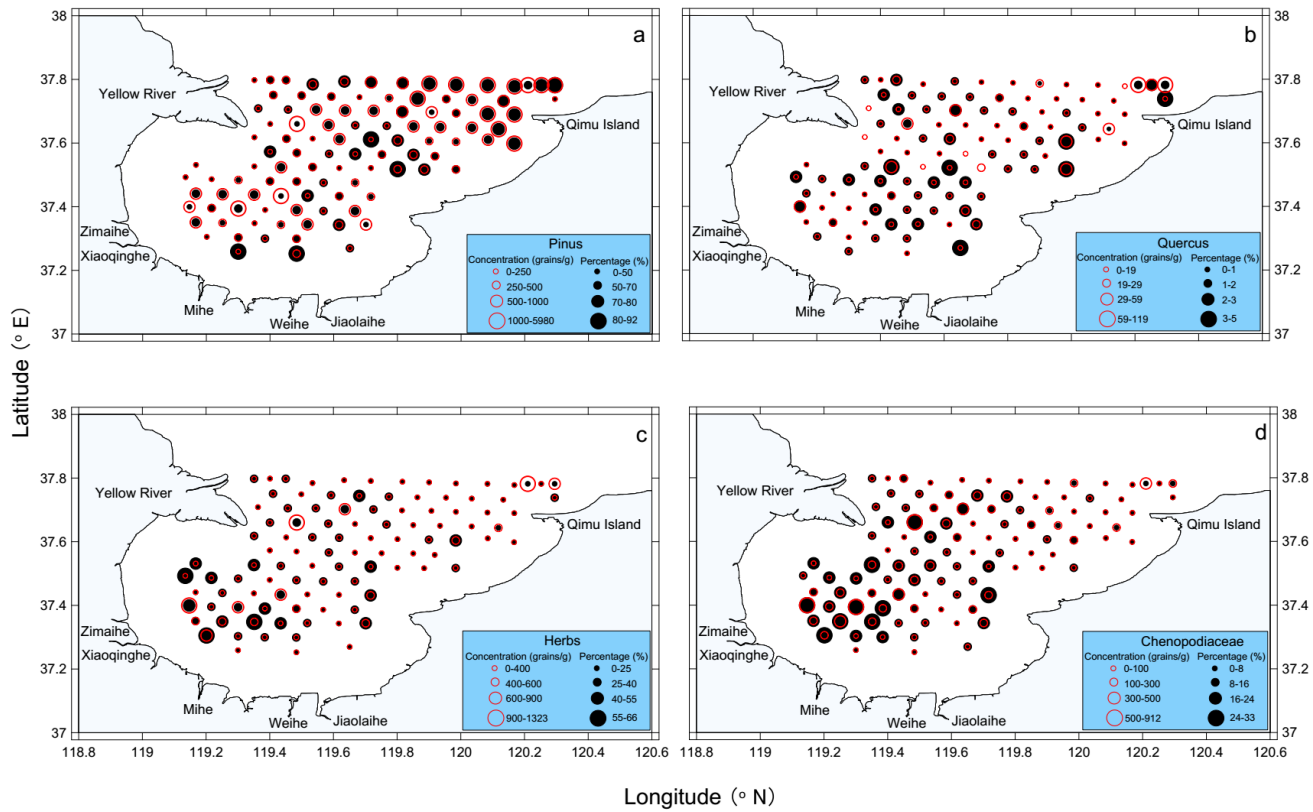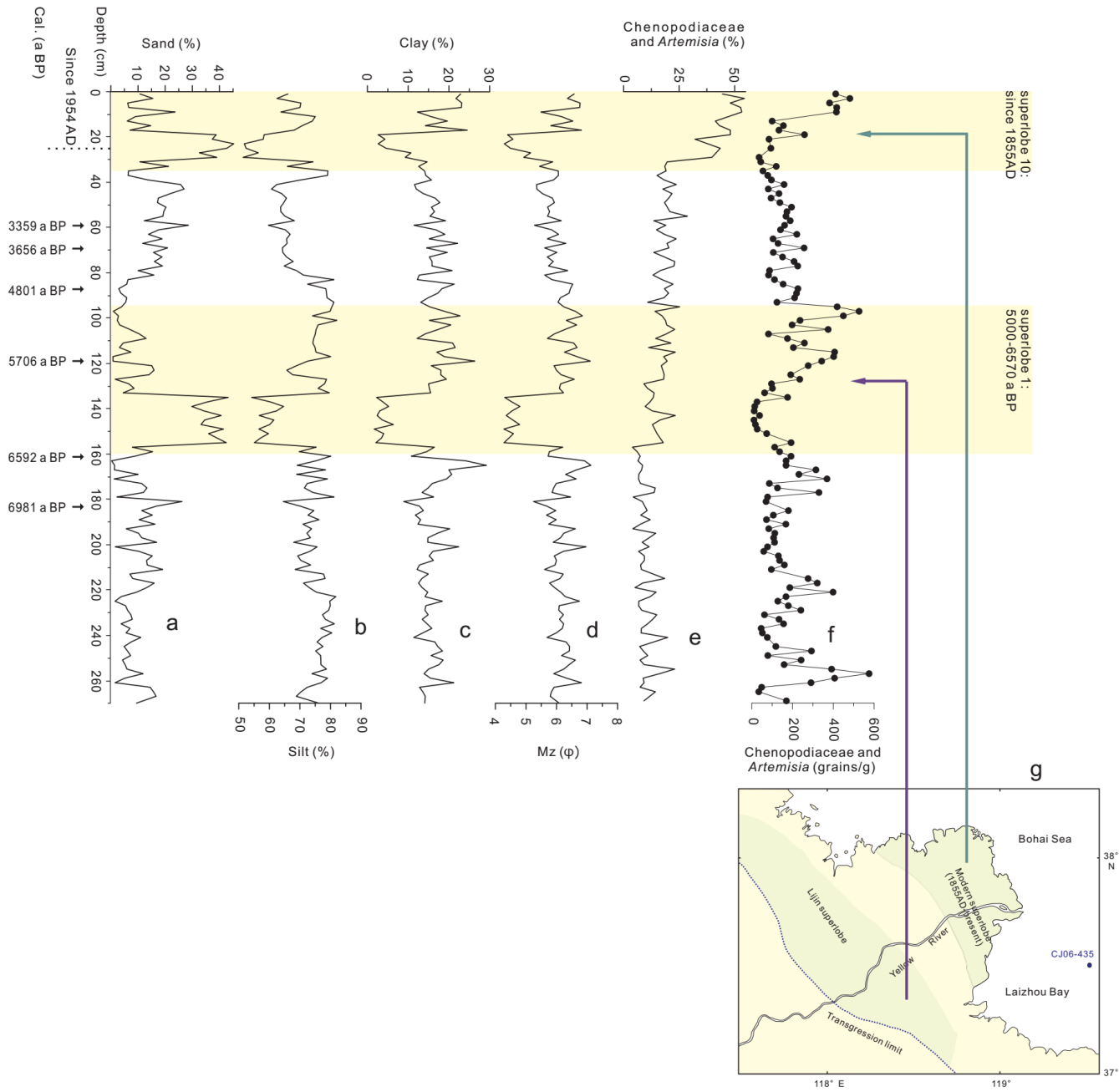Figure 6

1135

1136

1137

1138

1139

1140

1141

1142

1143

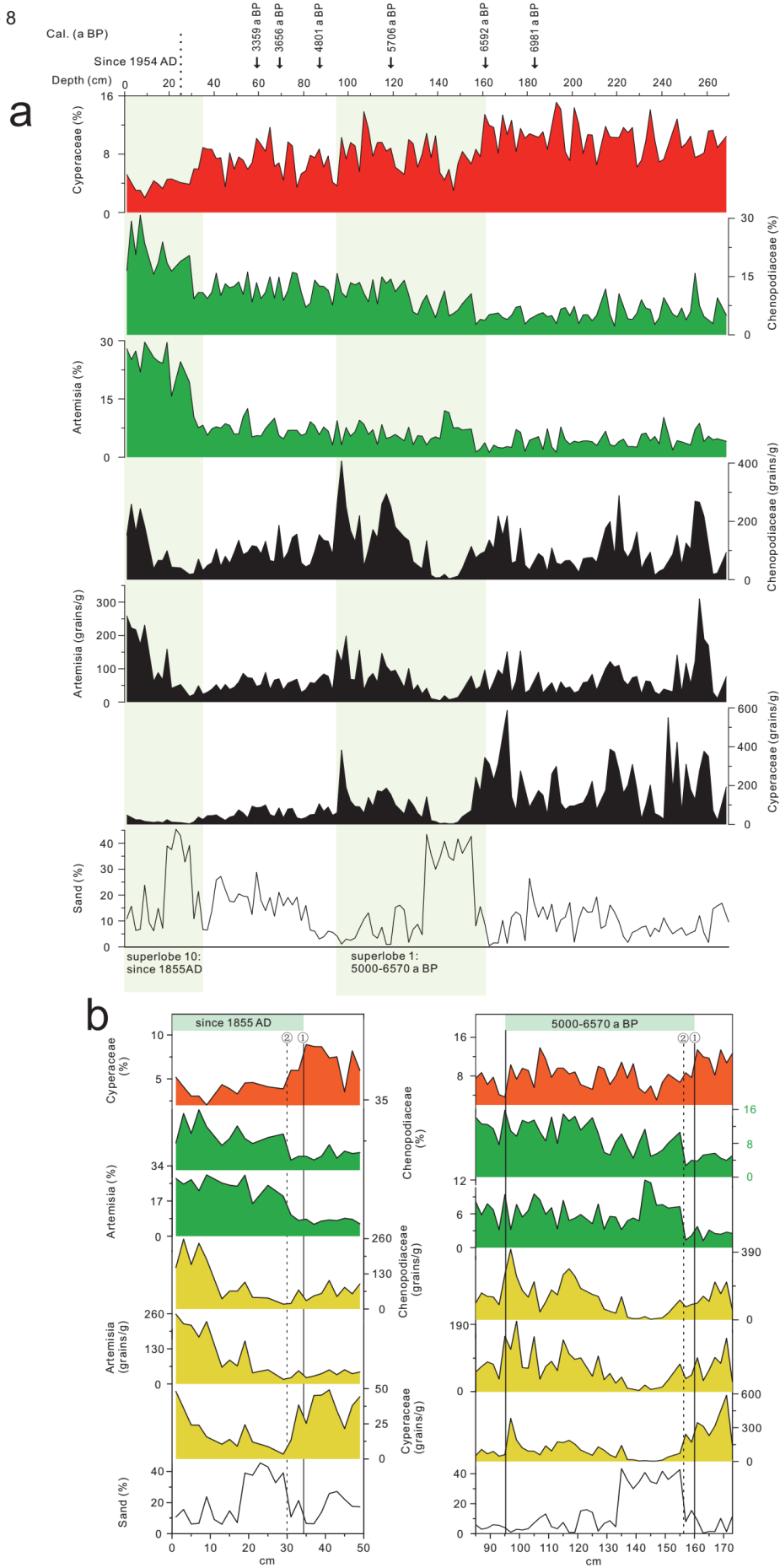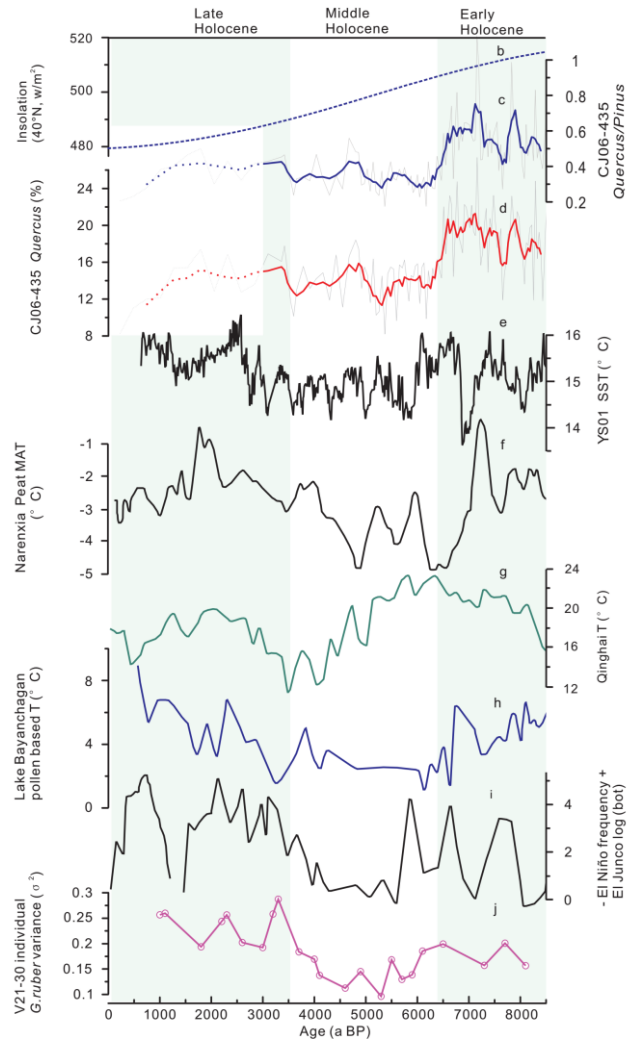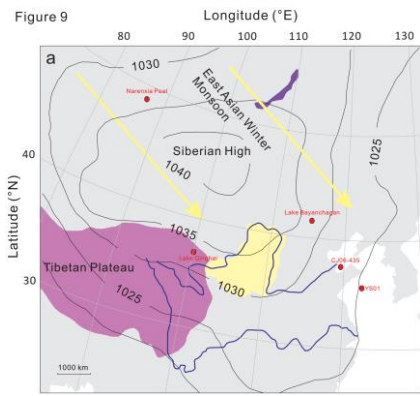1144

Figure 7

1145

1146

Figure 8

Figure 9

1148

1149

1150